The Thesis Committee for Michael Duncan Yoho
Certifies that this is the approved version of the following thesis:

Advancements in Coincidence Counting Experimental and Analytical Techniques for the Quantitative Detection of Low-Level Isotopes Relevant to Non-Proliferation Activities in High Dead-Time Applications

APPROVED BY
SUPERVISING COMMITTEE:

Supervisor: _____
Sheldon Landsberger

_____
Donivan R. Porterfield

Advancements in Coincidence Counting Experimental and Analytical Techniques for the Quantitative Detection of Low-Level Isotopes Relevant to Non-Proliferation Activities in High Dead-Time Applications

by

Michael Duncan Yoho, B.S.M.E.

Thesis

Presented to the Faculty of the Graduate School of

The University of Texas at Austin

in Partial Fulfillment

of the Requirements

for the Degree of

Master of Science in Engineering

The University of Texas at Austin

May 2015

Dedication

This work is dedicated to my parents, Blaine and Jean Yoho, for raising me right and also my fiancé, Neisla Rodriguez, for staying with me during those long nights at NETL.

Acknowledgements

This material is based upon work supported by the U.S. Department of Homeland Security under Grant Award Number, 2012-DN-130-NF0001. The views and conclusions contained in this document are those of the authors and should not be interpreted as representing the official policies, either expressed or implied, of the U.S. Department of Homeland Security.

I would like to thank Dr. Sheldon Landsberger for his faith in my potential to perform quality work in the field of radiochemistry, his hard work and support for my research, and his dedication to imparting to me a portion of his vast knowledge.

I would also like to thank the staff of the Nuclear Engineering Teaching Lab (NETL) including Larry Welsh, Mike Whaley, Tracy Tipping, and Mike Krause for their support of my research and willingness to teach me some of their knowledge in the field of nuclear engineering.

I would also like to acknowledge the contribution of many of the graduate students in the Nuclear Engineering Program at the University of Texas at Austin including Matt Montgomery for his help in modelling coincident gamma emissions and Siqiu Wang for her help in modelling the high-purity germanium (HPGe) detectors.

I would also like to thank Donivan R. Porterfield in the Actinide Analytical Chemistry Group (C-AAC) at Los Alamos National Laboratory (LANL) for his hard work and support of my research and for training me in the field of radiochemistry during my internship at LANL.

Abstract

Advancements in Coincidence Counting Experimental and Analytical Techniques for the Quantitative Detection of Low-Level Isotopes Relevant to Non-Proliferation Activities in High Dead-Time Applications

Michael Duncan Yoho, M.S.E

The University of Texas at Austin, 2015

Supervisor: Sheldon Landsberger

This thesis develops experimental and analytical procedures to detect trace amounts of isotopes of interest relevant to activities related to nuclear non-proliferation via γ-γ coincidence counting. By using multiple-detector systems, the time-correlated nature of γ-ray emissions of isotopes with complex decay schemes can be utilized to reduce background levels and interferences. This thesis is divided into five major sections. After a review of the state-of-the-art, system capability is presented by documenting the quantitative determination of selenium in neutron-activated fly ash. The complex fly-ash γ spectrum containing multiple interferences and high background levels constitutes a rigorous quality-assurance test of system performance and further simulates

the complex and difficult nature of fission-product spectra relevant to non-proliferation activities. Next, this thesis maps out system dead-time performance and presents a methodology to correct for dead-time in coincidence systems. This thesis then presents the experimental analysis of fission-product spectra generated via neutron activation in the TRIGA Mark II reactor at the University of Texas at Austin. Analytical procedures are presented to determine coincidence signatures and intensities, necessary for quantitative determination of any fission product via Monte Carlo techniques. Finally, the system's capability to quantify trace plutonium is examined, and a criterion is developed in order to determine the benefit of coincidence counting methodology for a specific isotope over standard nuclear counting techniques.

Table of Contents

List of Figures

List of Figures

List of Tables

Chapter 1: Introduction

Difficulties of time correlated γ detection

There are many difficulties associated with the acquisition and analysis of time correlated γ-emissions. First is the difficulty of predicting what energy signals will be detected for an isotope in question. A second issue is the need to determine coincidence detection efficiencies in order to determine quantitative activity levels. Finally, accurately correcting for dead-time, random-summing effects, random-coincidences, and self-attenuation all present difficulties above that which are presented by the conventional gamma spectroscopy methodology using a single detector. In conventional gamma spectroscopy, a standard procedure to determine concentrations of mono-energetic emitting nuclides such as ^{137}Cs is to count the dissolved sample material in a one L Marinelli beaker surrounding the HPGe. [1] recently used this technique to determine concentrations of ^{137}Cs and naturally occuring radioactive material (NORM) in sediment samples surrounding various reservoirs in Turkey. In that study, a standard containing mono-energic emitting nuclides was dilluted in a Marinelli beaker to determine an absolute counting efficiency. Other recent studies utilizing a similar methodology include determining ^{137}Cs concentrations in coniferous forests [2], and determining radioactive concentrations in air filters with Fukushima contamination [3]. Here, in place of a Marinelli beaker, the filters were wrapped around the detector endcap to achieve an optimum efficient counting geometry. The following discussion will attempt to

differentiate the difficulties of determining coincident γ-emission efficiencies from this standard methodology.

Theory of time correlated γ-emission

The thoery of radioactive decay presented in this section is primarily taken from the introduction to the Laboratoire National Henri Becquerel Table of Radionuclides [4], an excellent summary of the details of radioactive decay. The theory will be presented via a discussion of the decay of the fission-product ^{166m}Ho. Ho-166m is chosen due to its' having a sufficiently complex decay scheme to emphasize the involved problems of determining coincident γ-ray efficiencies.

Radionuclides disintgerate via the emission of β or α particles, electron-capture, spontaneous fission, or the emission of other single or multiple particles. For example, ^{166m}Ho decays via β^- emission 100% of the time. Depending on the energy of the β^- particle, the nucleus is left in either the ground or an excited state of the progeny isotope ^{166}Er. The decay structure of ^{166m}Ho is depicted in Figure 1. The various β^- transitions all have various probabilities, $P_\beta P_\beta$. The excited states of ^{166}Er then transition via either the emission of a γ-ray, internal-conversion (IC) of an electron, or in rare cases via electron-positron emission to a lower energy state.

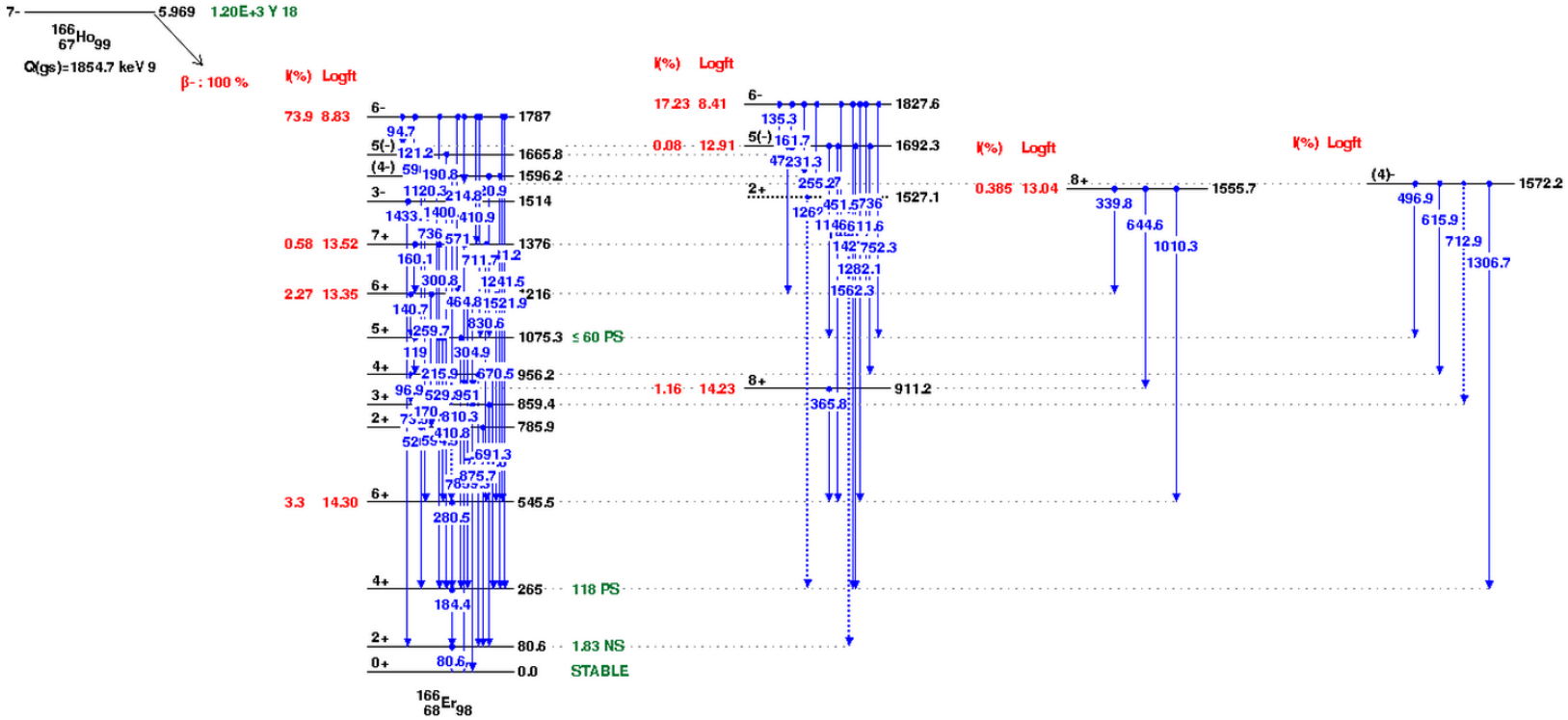

Figure 1: Decay scheme of ^{166m}Ho [5]

Sometimes transitions occur directly to the ground state and sometimes they create chains from one excited state to another until the ground state is reached, as is depicted in Figure 1. If the sum of the excited state half-lives in a particular decay-chain is less than or on the order of the coincidence timing gate of the detection systetm, then there is a probability that the counting system will register the energy deposition of one γ-ray in one detector and the energy deposition of a second γ-ray in another detector. In the case of ^{166}Er, all excited state half-lives are on the order of ps, whereas the timing resolution of the detection systems presented in this thesis are on the order of ns. In the case of ^{239}Pu decay to ^{235}U there exist transition half-lives on the order of ns to minutes in duration, ensuring the analyst must carefuly scrutinize the nuclear data for each isotope under consideration.

This thesis discusses three ways in order to determine coincidence intensities in order to quantitatively determine the quantitative isotopic activity of a sample of interest $A_{sam}A_{sam}$. The most accurate and simplest method utilizes a standard of the same isotope with known activity $A_{std}A_{std}$ counted in the same geometry and in the same matrix as the sample of interest. If counting times for sample and standard are equal and denoted by $t_{count}t_{count}$, and $C_{std}C_{std}$ and $C_{sam}C_{sam}$ are the counts in a certain coincidence peak for the standard and sample, respectively, then the coincidence intensity II in counts per dissintegration of the particular peak is given by Eq. 1 as

$$I = \frac{C_{std}}{A_{std} t_{count}} \quad \left[\frac{counts}{dissintegration}\right] \tag{1}$$

Note that in Eq. 1, the counting duration is assumed to be short compared to the isotope half-life. If this is not the case, then exponential decay during the count duration must be taken into account. The number of dissintegrations in the sample during the counting period is then given by Eq. 2.

$$Dissintegrations\ in\ sample = \frac{C_{sam}}{I} \tag{2}$$

A similar methodology to this is utilized in chapter 2 of this thesis.

In the analysis of fission product spectra for non-proliferation and material control & accountability applications, it may prove difficult to obtain certified standards of potentially dozens or more isotopes of interest. Further, it is a challenge to duplicate the same geometry and matrix density as the samples of interest. One way to overcome this challenge is by utilizing Monte Carlo methods. Recently, [6] developed a GEANT4 model of the time correlated γ-γ cascades of certain fission products. Experimental results of coincidence photo-peaks obtained via irradiation of ^{235}U varied from 71% lower to 45% higher than the simulated spectra. This thesis presents a similar methodology in Chapter 4 using MCNP simulations. Monte Carlo methods, while difficult to implement in practice for coincidence systems as indicated by the spread in accuracy in [6], have the potential to not only determine coincidence efficiencies necessary for quantitative results,

but also have the potential to quickly determine which isotopes have the potential to benefit from coincidence analysis. Further, in practice, it is a difficult task to even determine which coincidences from a certain nuclide will be present in the spectrum when faced with even a relatively simple decay scheme as in Figure 1. A drawback of the Monte Carlo based methodologies is there heavy reliance on the nuclear data which in some cases is incomplete. For example, current work being conducted at the Finnish IGISOL facility determining fission yields of ^{235}U via single γ detectors and coincidence systems that suffer from true coincidence summing (TCS) issues due to a close sample-detector geometry. For certain nuclides suffering from TCS, ground-state branching ratios were not located in the nuclear data [7].

As opposed to Monte Carlo techniques, a final method is to analytically determine coincidence intensities directly from the ENSDF files. A related task is determining coincidence counting intensities for the conventional γ-spectroscopy step of correcting for TCS effects in close-geometry applications. Indeed, the two tasks are so connected that [8] utilized coincidence counting in the HPGe clover at the Bhabha Atomic Research Center in Mumbai, India to determine TCS correction factors. Many algorithms exist to accomplish TCS corrections. One of the first algorithms presented in [9] utilizes recursive formulae for calculating emission probabilities. [10] improved upon the algorithm by adding in annihilation photon effects. [11] formalized these procedures by introducing a general matrix methodology. More recently, this matrix methodology has

been improved by [12] and [13] to include symbolic matrix manipulation and also inclusion of x-ray contributions for reverse-electrode HPGe detectors with relativly high detection efficiency at low energies. Commercial software such as GESPECOR [14] which utilizes Monte Carlo methods is readily available. A good review article of various TCS correction techniques has been previously published [15].

In order to present the reader with a sense of the difficulty of determining coincidence efficiencies and also self-attenuation corrections, a pseudo algorithm will be presented which utilizes similar methodologies to [9] and [11] to determine the detection efficiencies of ^{166m}Ho. The first step in determining coincidence efficiencies is listing all the decay paths and decay path probabilities for a particular isotope. For the β emitter ^{166m}Ho, the ENSDF files list all the β transition probabilities $P_\beta P_\beta$. It also lists the total transition probability for level ii to level jj including γ and conversion electron probabilities:

$$P_g(i,j) = I_\gamma(i,j) + I_{CE}(i,j) \tag{3}$$

From this list of levels and transitions, a directed-acyclic graphical model can be generated. Figure 2 depicts a model of ^{166m}Ho decay. With the graphical model, a list of all the 228 decay paths of ^{166m}Ho can then be generated with a basic algorithm such as a modified depth-first search [16]. The conditional transitional probabilities from level ii to level jj given it is on path QQ can be found by the expression

$$P_g(i,j)|Q = \frac{P_g(i,j)}{\sum_{\forall j' \neq j} P_g(i,j')} \quad (4)$$

Now that the conditional transition probabilities have been found, total probability for path kk can be found by multiplying the ββ transition probability to decay path QQ by all the conditional transition probabilities along the path which is given by the expression

$$P(path\ Q) = P_\beta(Q) * \prod_{\forall transitions\ in\ Q} P_g(i,j)|Q \quad (5)$$

In order for one γ-ray to deposit its full energy in one detector and another γ-ray located on the same decay path to deposit its full energy in a second detector of a two-detector coincidence system and register a coincidence, many things must happen. First, both transitions in question must emit γ-rays and not de-excite via IC. The probability of a transition ii emitting a γ-ray is given by

$$\frac{1}{1 + \alpha_{T,i}} \quad (6)$$

where $\alpha_{T,i}\alpha_{T,i}$ is the total conversion coefficient for transition ii. Next, both γ-rays must be detected in both detectors. The probability of a γ-ray being detected is given by

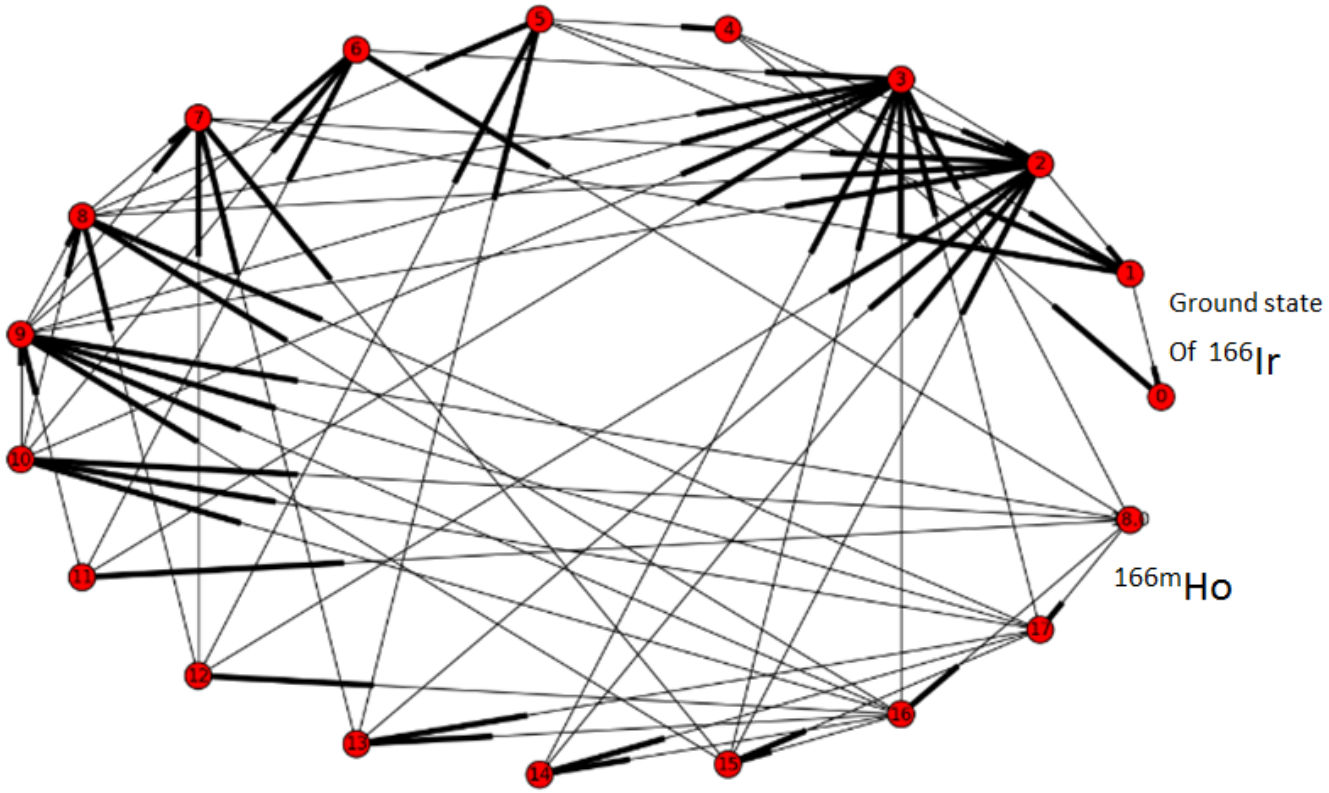

Figure 2: Graphical model of ^{166m}Ho decay decay chains

the full-peak efficiency at energy ii: $\varepsilon_i\varepsilon_i$. Both detectors will be assumed to have the same efficiency with the source equidistant from both detector endcaps. Further, other transitions along the path kk must not emit any γ-rays, x-rays from K or L shell de-excitations following the emission of a conversion electron, or x-rays following de-excitation from subsequent Auger electrons which may deposit any energy in either detector. Note that when finding the probabilities of the detectors not registering any energy deposition by these auxilliary particles, total efficiencies $\varepsilon_i^T\varepsilon_i^T$ must be used. Total efficiencies may be found either via Monte Carlo simulation [17] or via the use of a peak-to-total calibration kit [18]. A general method to find the coincidence probability per decay P(A, B)P(A, B) for γ-ray A and γ-ray B is then given by the following expression:

$\forall\ paths\ Q\ \in\ decay\ structure\ of\ isotope\ of\ interest$:

if $transition_A \in k$ and $transition_B\ \in Q$if $transition_A \in k$ and $transition_B\ \in Q$:

$$P(A,B) \leftarrow P(A,B) + (\varepsilon_A)\left(\frac{1}{1+\alpha_{T,A}}\right)(p_{path})(\varepsilon_B)\left(\frac{1}{1+\alpha_{T,B}}\right)(p_{path}k)\prod_{\forall i\neq A,B}\{P(A,B) \leftarrow$$

$$P(A,B) + (\varepsilon_A)\left(\frac{1}{1+\alpha_{T,A}}\right)(p_{path})(\varepsilon_B)\left(\frac{1}{1+\alpha_{T,B}}\right)(p_{path}k)\prod_{\forall i\neq A,B}\{$$

$$+\left(\frac{\alpha_{K,j}}{1+\alpha_{T,j}}\right)\left\{\omega_K\left(1-\varepsilon_K^T\right)^2\left[\bar{w}_L n_{KL}\left(1-\varepsilon_L^T\right)^2 + n_{KL}\left(1-\bar{w}_L\right) + \left(1-n_{KL}\right)\right] +\right.$$

$$\left.\left(1-w_K\right)\left[n_{KL}\bar{w}_L\left(1-\varepsilon_L^T\right)^2 + n_{KL}\left(1-\bar{w}_L\right) + \left(1-n_{KL}\right)\right]\right\} \quad +$$

$$\left(\frac{\alpha_{K,j}}{1+\alpha_{T,j}}\right)\left\{\omega_K\left(1-\varepsilon_K^T\right)^2\left[\bar{w}_L n_{KL}\left(1-\varepsilon_L^T\right)^2 + n_{KL}\left(1-\bar{w}_L\right) + \left(1-n_{KL}\right)\right] + \right.$$

$$\left.\left(1-w_K\right)\left[n_{KL}\bar{w}_L\left(1-\varepsilon_L^T\right)^2 + n_{KL}\left(1-\bar{w}_L\right) + \left(1-n_{KL}\right)\right]\right\}$$

$$+\left(\frac{\alpha_{L,j}}{1+\alpha_{T,j}}\right)\left[\bar{w}_L\left(1-\varepsilon_L^T\right)^2 + \left(1-\bar{w}_L\right)\right] + \left(\frac{\alpha_{L,j}}{1+\alpha_{T,j}}\right)\left[\bar{w}_L\left(1-\varepsilon_L^T\right)^2 + \left(1-\bar{w}_L\right)\right]$$

$$+\left(\frac{\alpha_{M,j}}{1+\alpha_{T,j}}\right) + \left(\frac{\alpha_{M,j}}{1+\alpha_{T,j}}\right) \}$$

(7)

In the above expression $\alpha_k\,\alpha_k$, $\alpha_L\alpha_L$ and $\alpha_M\alpha_M$ are the coefficients for K, L, and M electron conversions, respectively. Further, $\omega_K\omega_K$ is the probability that a K-shell vacancy will emit a K x-ray; $1\text{-}w_K 1\text{-}w_K$ is the probablity that a K-shell hole will emit a K Auger electron; $n_{KL}n_{KL}$ is the overal probability that a K-shell hole will produce an L-shell hole; $\varepsilon_K^T\varepsilon_K^T$ is the total efficiency associated with a K x-ray assuming the efficiency is relatively constant for all K x-rays; $\varepsilon_L^T\varepsilon_L^T$ is the total efficiency associated with an L x-ray; and $\bar{w}_L\bar{w}_L$ is the average probability that an L-shell hole will emit an L x-ray.

Eq. 7 demonstrates one of the key trade-offs with coincidence counting. Note that one of the major components of the coincidence probability is the multiplication of the detector efficiencies for both γ-ray energies $\varepsilon_A\varepsilon_A$ and $\varepsilon_B\varepsilon_B$. Everything else in the expression deals with relatively minor effects due to the simultaneous deposition of

energies from x-rays and other γ-rays along the path. Therefore, an order-of-magnitude estimate of coincidence intensity is given by the simplification:

$$P(A,B) \approx \sum_{\forall paths\ containing\ A,B} p(path)\varepsilon_A\varepsilon_B \tag{8}$$

In conventional γ-spectroscopy, the detection efficiency for γ-ray A is roughly given by

$$P(A) \approx \sum_{\forall paths\ containing\ A} p(path)\varepsilon_A \tag{9}$$

If the number of paths containing γ-rays A and B is equal to one, then the ratio of the standard, one-detector efficiency divided coincidence efficiency, α, is approximated by

$$\alpha = \frac{efficiency(single\ detector\ method)}{efficiency(coincidence\ method)} \approx \frac{\varepsilon_A}{\epsilon_A\epsilon_B} = \frac{1}{\epsilon_B} \tag{10}$$

Eq. 10 demonstrates that, to within an order of magnitude approximation, the ratio of the efficiency of a coincidence system to the efficiency of a one-detector system is given by the reciprocal of the efficiency of the second γ-ray in question. One major assumption to Eq. 10 is a perfect correlation between both γ-rays where both γ-rays always occur on the same path. Given this assumption, Eq. 10 represents an upper-bound for coincidence performance as compared to standard γ-spectroscopy methodologies utilizing a single detector. In any case, Eq. 10 demonstrates the maxim of coincidence counting: *detector efficiencies should be maximized by placing the sample as close as possible to both*

detector endcaps. Another insight which may be taken from Eq. 10 is that coincidence methodologies work better for isotopes emitting high abundance γ-rays around the most efficient energies for the detectors being used. For a typical coaxial HPGe detector without a Be or C thin window, the maximum efficiency typically lies between 100 to 200 keV, as demonstrated by an efficiency curve in Figure 3 generated via a ^{166m}Ho source.

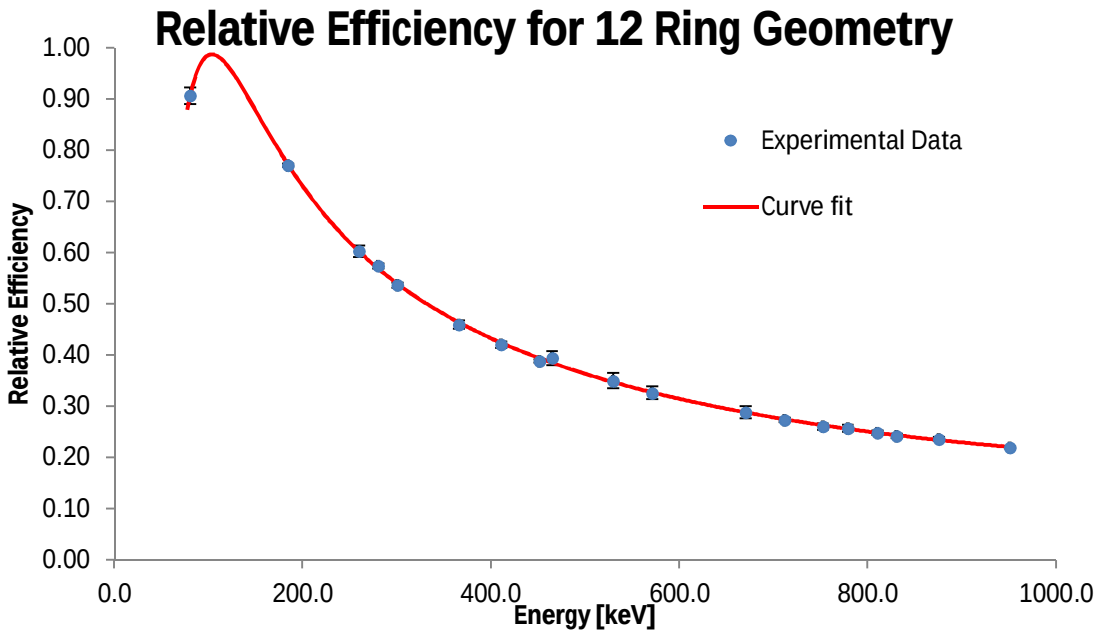

Figure 3: Relative efficiency curve for a 40% relative efficiency coaxial HPGe

Eq. 10 also demonstrates the trade-off associated with coincidence counting. As will be demonstrated in the following chapters, coincidence counting has the potential to drastically reduce background levels and spectral interferences. However, this comes at

the cost of lowered overall detection efficiency. For example, ^{239}Pu is being analyzed for stockpile stewardship activites with typical intense γ-ray and x-ray energies around 90 to 205 keV. If counting geometry is optimized and two very efficeint detectors are used with around 20% full-peak efficiencies at the energies in question, Eq. 10 demonstrates that at best, net coincidence peak counts will be reduced by a factor of five. Therefore, background levels and interferences must be reduced substantially in order to have a real improvement in counting statistics.

Eq. 7 assumes an isotropically emitting point source. In order to negate these assumptions, then Eq. 7 must be integrated over the volume of the source. In the sister-problem of correcting for TCS effects in a single detector, correction for volume sources has been achieved via the introduction of a third efficiency curve taking into account the variation of the detector efficiency over source volume [19].

When an nucleus de-excites via internal conversion or γ emission, angular momentum must be conserved. The emitted γ-ray will therefore have the angular momentum equal to the difference in angular momentum between the parent and progeny nuclear levels. In a decay path containing two γ-ays $A \rightarrow B \rightarrow CA \rightarrow B \rightarrow C$, the particular angular momenta of the two γ-rays necessitates an angular correlation $W(\theta)W(\theta)$ which must be taken into account in order to achieve accurate results if coincidence efficiencies are calculated analytically or via Monte Carlo methods. The theory of angular correlation is well established [20], with the angular correlation function given as

$$W'(\theta) = 1 + \left(\frac{R}{Q}\right)\cos^2(\theta) + \left(\frac{S}{Q}\right)\cos^4(\theta) \tag{11}$$

where R/QR/Q and S/QS/Q are tabulated coefficients which depend on the angular momentum of states AA, BB, and CC and the multipolarity of the two γ-rays. The tabulated coefficients in [20] normalize Eq. 10 to θ = 90°θ = 90°. Therefore, Eq. 11 must be normalized to the average angular correlation from θ = 0θ = 0 to θ = πθ = π in order to acquire a useable correction factor. This process gives

$$W(\theta) = \frac{1 + \left(\frac{R}{Q}\right)\cos^2(\theta) + \left(\frac{S}{Q}\right)\cos^4(\theta)}{\frac{1}{\pi}\int_0^{\pi} d\theta\left[1 + \left(\frac{R}{Q}\right)\cos^2(\theta) + \left(\frac{S}{Q}\right)\cos^4(\theta)\right]} \tag{12}$$

For example, in ^{60}Co decay the electric quadropole (E2) 1173.2 keV γ-ray is emitted from a 4+ spin and parity level. The nucleus then reaches a 2+ level and in turn emits a second E2 1332.5 keV to reach ground at 0+. This information is used to find the angular correlation coefficients tabulated in [20]. The correlation of the 1173 and 1332 keV γ-rays of ^{60}Co decay is then given by

$$W'(\theta) = 1 + \frac{1}{8}\cos^2(\theta) + \frac{1}{24}\cos^4(\theta) \tag{13}$$

A plot of Eq. 13 is given in Figure 4.

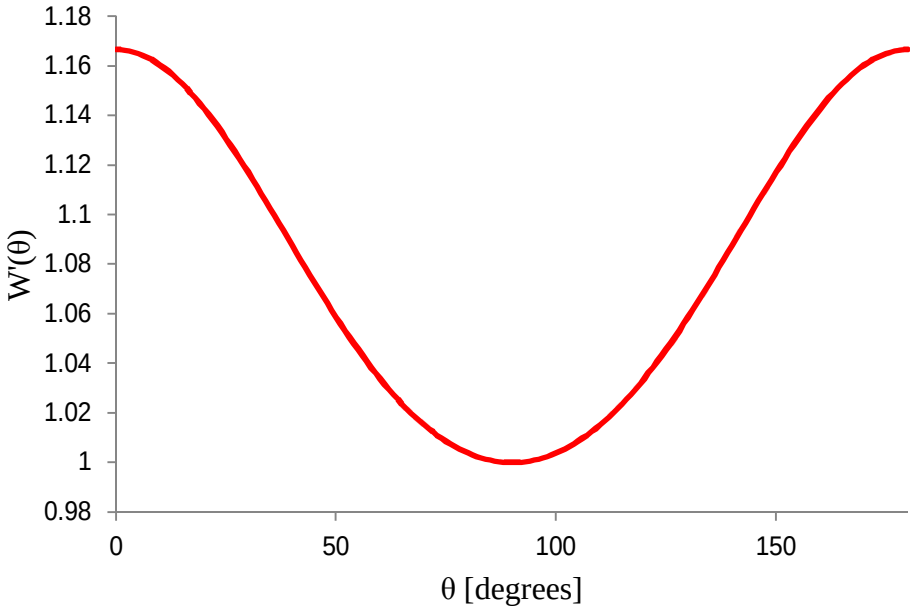

Figure 4: Angular correlation of 1332.5 and 1173.2 γ-rays of ^{60}Co decay

A complication exists when a level transition contains mixed electric and magnetic multipolarities. The mixing ratio $\delta^2 = \mathrm{E_{L+1}/M_L}\delta^2 = \mathrm{E_{L+1}/M_L}$ is usually tabulated in the ENSDF files for each well-studied level transition [4]. Using $\delta^2\delta^2$, a simple average correlation can be then computed according to

$$\overline{W(\theta)} = \frac{1}{1+\frac{1}{\delta^2}} W_E(\theta) + \frac{1}{\delta^2+1} W_M(\theta) \qquad (14)$$

To accurately calculate coincidence efficiencies, not only the primary two γ-ray efficiencies in Eq. 7 must be multiplied by the angular correlation, but also all of the auxilliary γ-rays in the decay chain which may deposit energies in either detector.

Further, if the angular correlation is not included in the Monte Carlo generation of particle tragectories, then $W(\theta)W(\theta)$ should be integrated over the solid-angles subtended by the source and detectors and weighted by the efficiency function accross the face of the detectors. If large, highly efficient detectors are utilized, then these angular correlation corrections may be mitigated as detector geometry approaches 4π as in a dual clover geometry.

A further complexity associated with analytically determining coincidence intensities is accounting for self-attenuation in the sample. For example, for stockpile stewardship applications, heavy metal samples containing high-z materials such as uranium and plutonium will substantially attenuate the γ-rays. Therefore, every single term in Eq. 7 must be multiplied by a self-attenuation factor and integrated over the volume of the source. With such complexities facing the coincidence analyst conducting stockile stewardship and non-proliferation activities, analytically determining γ-γ coincidence absolute detection efficiencies is a formidable task.

Coincidence performance criterion

The previous discussion derived an upper-bound for α, the ratio of the γ-γ coincidence intensity to an intensity measured with a single γ-detector. Using principles of basic counting statistics, this ratio can be elaborated upon to derive an expression for a cut-off point for the net peak-to background ratio in the normal spectrum where

coincidence counting will yield a more accurate result. The formula is based on the following scenario. A γ spectroscopist routinely determines concentrations for an isotope in a counting duration which typically yields a number of net photopeak counts $C_\gamma C_\gamma$ and background counts B. No spectral interferences are present. The question is whether γ-γ coincidence can determine the isotope concentration in the same amount of time with a better relative uncertainty.

As will be demonstrated in the following chapters, γ-γ coincidence counting has the potential to virtually eliminate background levels. Therefore, for the purposes of deriving a theoretical lower-bound, coincidence background levels will be negligible, and the percent uncertainty of the coincidence counts is given bygible

$$100 * \frac{\sigma_{C_{\gamma\gamma}}}{C_{\gamma\gamma}} = 100 * \frac{\sqrt{C_{\gamma\gamma}}}{C_{\gamma\gamma}} \tag{15}$$

The uncertainty of the conventional single detector spectrum is arrived at by adding in quadrature the full-peak area uncertainty and the background uncertainty:

$$100 * \frac{\sigma_{C_\gamma}}{C_\gamma} = 100 * \frac{\sqrt{\left(\sqrt{C_\gamma + B}\right)^2 + \left(\sqrt{B}\right)^2}}{C_\gamma} = 100 * \frac{\sqrt{C_\gamma + 2B}}{C_\gamma} \tag{16}$$

In order for the coincidence method to be superior

$$100 * \frac{\sqrt{C_{\gamma\gamma}}}{C_{\gamma\gamma}} < 100 * \frac{\sqrt{C_\gamma + 2B}}{C_\gamma} \tag{17}$$

Simplifiying this expression and substituting in $\alpha = \frac{C_\gamma}{C_{\gamma\gamma}} \alpha = \frac{C_\gamma}{C_{\gamma\gamma}}$ gives

$$\frac{B}{C_\gamma} > \frac{\alpha - 1}{2} \tag{18}$$

Say the analyst is debating the implementation of a γ-γ coincidence system which reduces net-peak areas by a factor of $\alpha = 10 \alpha = 10$ but will elminate background. In order to justify this technique, the present background must be $\frac{B}{C_\gamma} > \frac{10\text{-}1}{2} > 4.5 \frac{B}{C_\gamma} > \frac{10\text{-}1}{2} > 4.5$ times higher than the net peak areas currently examined. Substituting Eq. 10 for the upper-bound for coincidence efficiency and assuming there exists two perfectly correlated γ-rays at similar energies gives

$$\frac{B}{C_\gamma} > \frac{\frac{1}{\varepsilon_B} - 1}{2} \approx \frac{1}{2\varepsilon_B} \tag{19}$$

Now, say the analyst can manipulate system geometry in order to achieve around 10% full-peak efficiency for the γ-rays in question. Then the ratio of the current backround to the current single detector net photopeak counts must be greater than $\frac{B}{C_\gamma} > \frac{1}{2*0.1} =$ $10 \frac{B}{C_\gamma} > \frac{1}{2*0.1} = 10.$

Conclusions

This introduction has overviewed some of the basic physical principles underlying time correlated γ-ray detection. Some of the fundamental problems facing the coincidence analyst have been presented including determining coincidence efficiencies, correcting for angular-correlations, and correcting for self-attenuation. Three methods have been discussed for determining coincidence efficiencies. The comparator method given by Eqns. 1 and 2 is most accurate and easily implemented when standards in the exact geometry and matrix as the material in question are readily available. If acquiring such a standard proves impossible, then Monte carlo methods as discussed in Chapter 4 of this thesis and in [6] may be utilized. The final alternative is to analytically determine coincidence intensities utilizing a methodology similar to the pseudo code depicted in Eq. 7.

It has been demonstrated that to within an order-of magnitude approximation, an upper-bound on coincidence performance compared to methodologies utilizing a single detector is equal to the full-peak efficiency of the energy of the second γ-ray in question. It has also been demonstrated that coincidence performance compared to single detector methodologies is optimal for counting γ-rays at the most efficient energies for the detection system being utilized. Finally, the formula Eq. 18 has been developed to aid the

gamma spectroscopist in the decision of whether or not to implement a coincidence system.

Chapter 2: Determination of Se in coal fly ash

Abstract

The determination of Se in fly-ash via neutron activation poses difficulties to the gamma spectroscopist due to high Compton backgrounds as well as interference peaks from the ^{180}Hf(n, γ)^{181}Hf and ^{181}Ta(n, γ)^{182}Ta activation products. A methodology is presented to eliminate these interferences in geological samples via γ-γ coincidence. The methodology includes experimentally correcting for dead-time and random-summing. Random-coincidence gains which may lead to an over-estimation of concentration are corrected via post-acquisition analysis of the list-mode data. Experimentally determined Se concentrations in fly ash and other geological and biological reference materials agreed very well with the certified values. The complex neutron activated fly-ash spectrum with high background levels and interferences simulates the difficult nature of a fission-product spectrum. Therefore, this Chapter presents a rigorous test case for the capability of a γ-γ coincidence system to quantitatively determine isotopic concentrations in non-proliferation applications.

Introduction

The strong coincidence between the 136 and 264 keV γ-rays of neutron activated ^{75}Se makes this radionuclide an ideal candidate for instrumental neutron activation analysis (INAA) combined with a coincidence detection system. A prior study determined selenium concentrations in biological materials using a high-purity germanium (HPGe) detector combined with an active NaI(Tl) shield creating a timing-gate [21]. A combination of anti-coincidence and coincidence timing gates with two HPGe and one NaI(Tl) active shield was used in a previous study [22]. However, geological samples contain interferences not present in biological materials. The primary 136 and 264 keV γ-rays associated with neutron activated ^{75}Se in geological samples suffer from interferences from the 136 keV and 264 keV γ-rays of ^{181}Hf and ^{182}Ta, respectively. Further, the 136 keV γ-ray from ^{181}Hf is always emitted in coincidence with a 346 keV level-transition. The ^{182}Ta 264 keV γ-ray transition does not decay directly to ground but is always emitted in coincidence with one of five other transitions, most prominently the most intense 67 and 1189 keV transitions. Therefore, coincidence systems utilizing only timing windows will not completely eliminate these interferences.

Previously selenium concentrations were determined by employing Ge(Li) detectors with analog electronics to put energy gates on the 136 and 264 keV ^{75}Se photo-peaks in fly ash [23]. This procedure effectively eliminated the ^{181}Hf and ^{182}Ta interferences. The present work elaborates on this procedure by presenting a coincidence

methodology that finds three-dimensional coincidence peak volumes from the list mode data with dead-time, random-summing, and random-coincidence corrections. In particular, many types of neutron activated geological specimens have high dead-times which necessitates proper correction which may not be taken into account with two detectors. As previously discussed [24], coincidence techniques improve sensitivity via background reduction at the cost of efficiency. Therefore, coincidence techniques are well suited for measurements in a high gamma-ray background. Further, limited resources and demand for detector time necessitate that sample turn-around time be as short as possible. These two facts suggest that coincidence counting of ^{75}Se in fly ash should occur at moderate dead-times to maximize throughput.

This increase in sample activity leads to possible random coincidences in addition to true coincidences inside the peak volumes which will lead to an overestimation of analyte concentration in the sample. Methodologies have been presented to correct for random coincidences including reduction techniques [25] and by examining the diagonal Compton ridge-lines in the two-dimensional histogram [26]. Another study used a separate analog amplifier and discriminator with a long time delay to record only random-coincidences for a BGO Compton suppression system [27] and [28]. A similar methodology is presented in this work where a time delay is placed post-acquisition on the list-mode data to reproduce the random coincidence two-dimensional histogram. The random coincident peak-volumes are then subtracted from the total coincidences to get the true coincidence count-rate. Dead time and random-summing correction for the

coincidences in the two-detector system is accomplished via the use of a uniform pulser. It is established that systematic bias in using uniform pulses as opposed to random pulses are negligible if pulse count-rate is negligible in comparison to total sample count-rate [29], as is the case in the present study. The present work also outlines system set-up, optimization and data-analysis in a straightforward manner with the hopes of demonstrating the relative ease of implementing list-mode γ-γ coincidence spectroscopy.

Experimental

Sample preparation

One sample of each of six NIST certified reference materials consisting of coal fly ash (1633a and 1633b), bituminous coal (1632d), bovine liver (1577b), oyster tissue (1566a), and typical diet (1548a) were irradiated for four hours at 4.5×10^{12} cm^{-2} s^{-1} neutron flux in the TRIGA Mark II reactor depicted in Figure 5 along with a 9.92(8) μg/g concentration of a selenium standard. Reference material and standard weights ranged from 0.25 to 0.50 g in order to maintain constant volume to achieve nearly identical neutron flux profiles. Activity in the samples was allowed to decay for two weeks prior to counting to reduce backgrounds and dead time associated with short-lived activation products. Samples and standards were then counted for 24 hours laboratory time each.

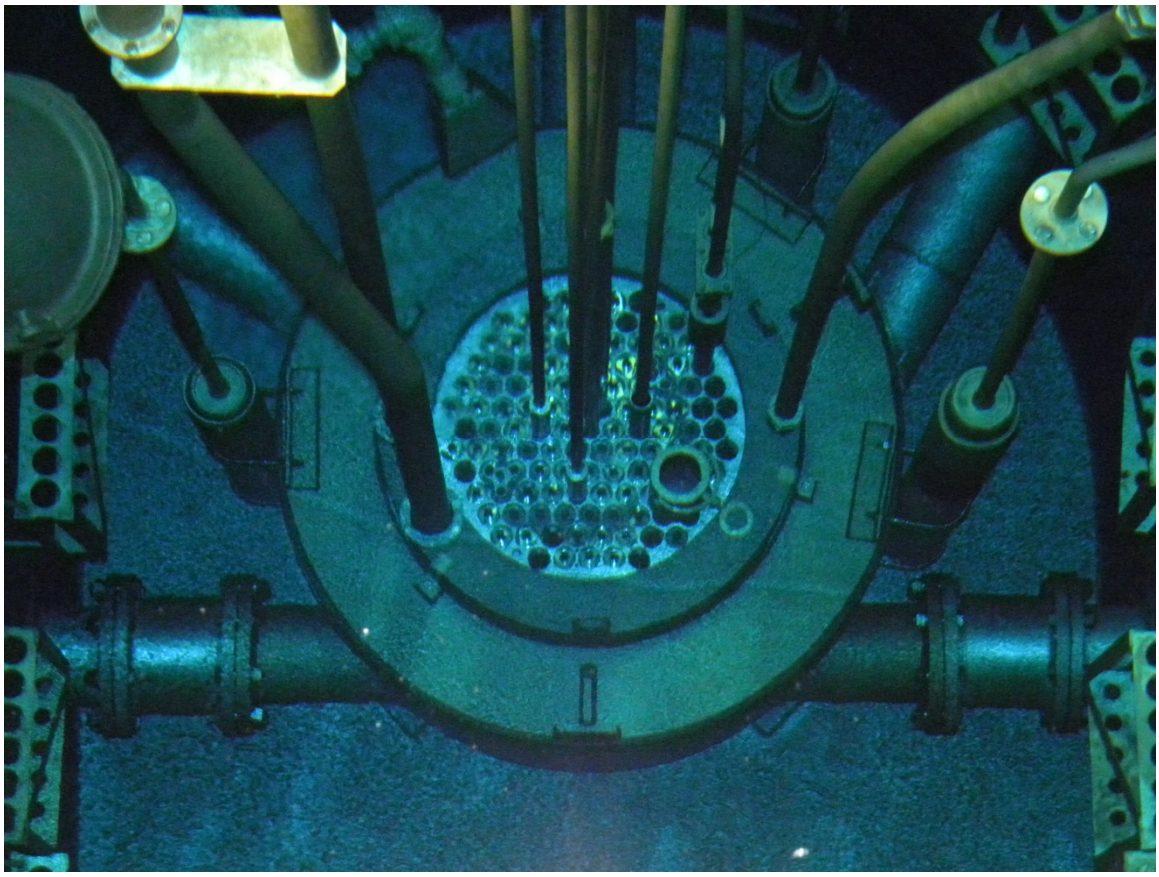

Figure 5: Core of TRIGA Mark II reactor at UT Austin

Detection system

The coincident detection system consists of a 35% relative efficient coaxial Canberra HPGe model GR3519 S/N 03036201 and a 50% relative efficient coaxial Ortec HPGe model GMX50P4-83 S/N 50-TN42071A. The system is surrounded by a 5 in lead shield and 6 in radius passive NaI(Tl) scintillator not used in this experiment. The detector energy outputs are connected to an XIA PIXIE-4 digital-signal-processor (DSP)

[30]. The detectors are situated at 180° and sample centers are at a one cm distance from each endcap. The optimization of the trapezoidal shaping time and flat-top have been covered in [31], [32] and [33]. An energy shaping time of 8 μs for both detectors was chosen in order to optimize energy resolution. The energy trapezoidal flat-top times for both detectors were set at the pre-amplifier output rise times of 0.7 μs obtained via oscilloscope inspection, depicted in Figure 6, of pulses generated by a ^{60}Co source.

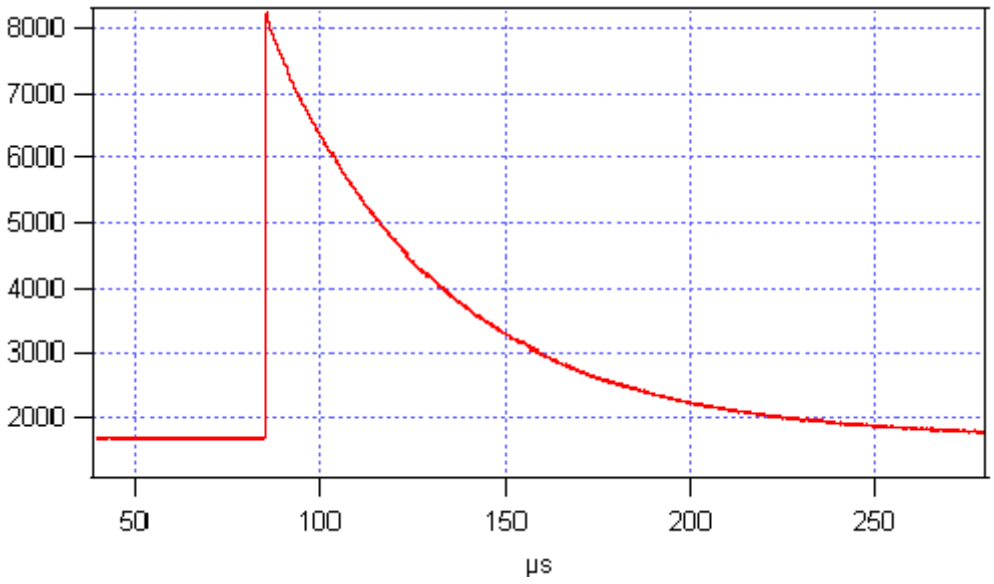

Figure 6: ^{60}Co pre-amplifier pulse shape for HPGe detector

Other DSP parameters, including fast-filter times for random summing correction, were set at factory values. With these parameters, the Canberra and Ortec full-width-half-max (FWHM) resolutions at 1332.5 keV with ^{60}Co were measured as 2.2 and 2.0 keV, respectively. DSP quality was verified by comparing these resolutions to optimal resolutions obtained with an analog Ortec 672 amplifier and 921E multi-channel-analyzer

(MCA). Resolutions are consistent between analog and digital systems, as well as with the detector certification sheets. The Ortec HPGe generates a significant left tail in its photo-peaks due to defects created in the crystal manufacturing process, as noted in the certification sheet. An image of the coincidence system is depicted in Figure 7.

The DSP was set to record list-mode data containing the voltages and time-stamps of detector pulses from either one or both detectors within a specified timing window capable of generating both singles and two-dimensional histograms. The timing window was selected by placing a coincident γ-emitting ^{60}Co source one cm from each detector end-cap and collecting list-mode data for 10 minutes. A weak ^{60}Co source was selected so the data only contained true coincidences between the 1173.2 and 1332.5 keV γ-rays. The average time between coincidences was determined to be 15 ns with a standard deviation of 155 ns. The timing window was set as small as possible at ±500 ns in order to minimize the number of random coincidences recorded but still include three standard deviations of true coincidences.

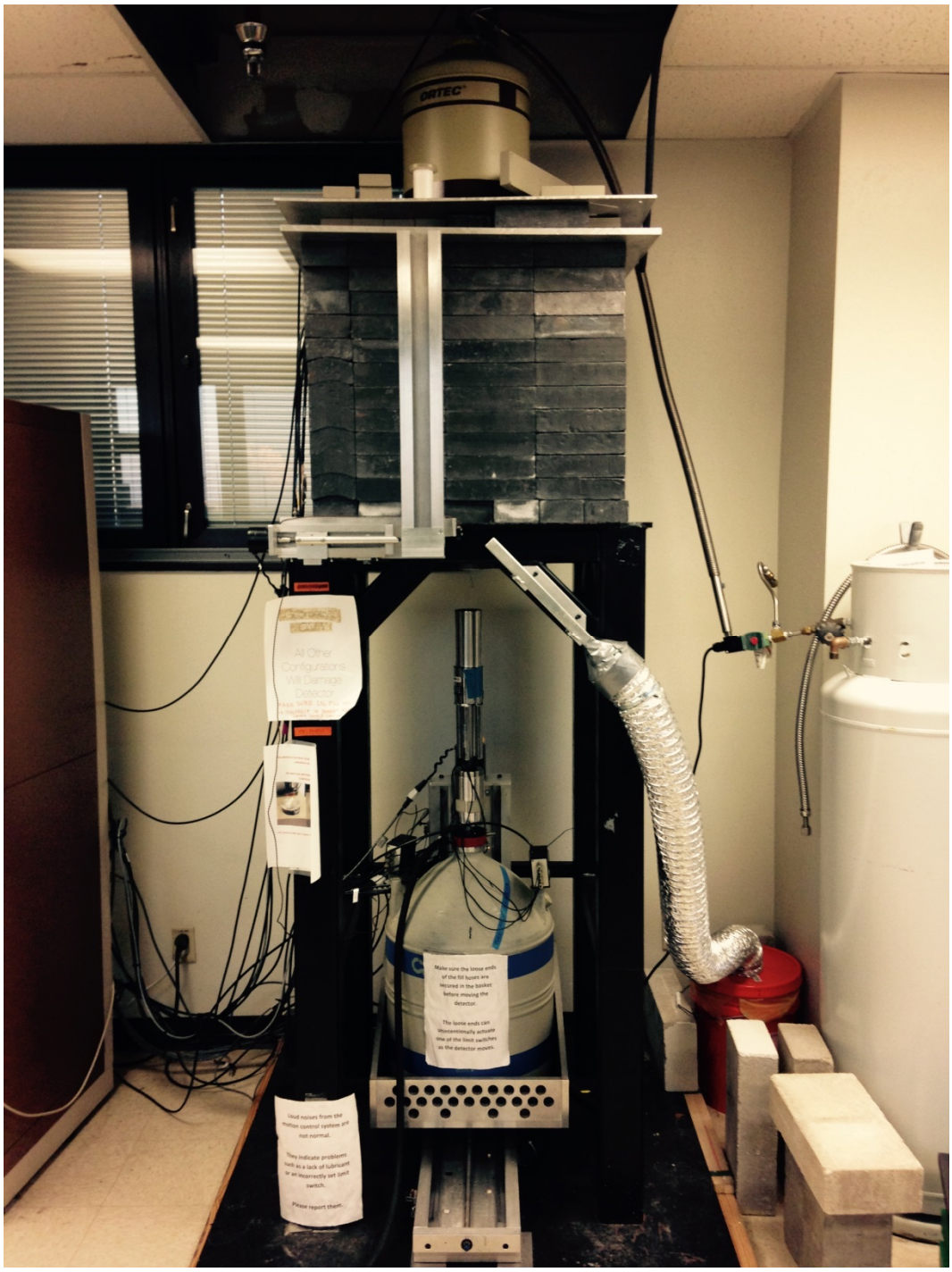

Figure 7: Coincidence system used in Se analysis

List mode data coincidences were stored in an 8192x8192 histogram, with each histogram cell containing the number of coincidences which occurred at the specified detector one (Ortec) and detector two (Canberra) inputs. DSP voltage gains were set in order for the histogram to span an energy range from 0 to 3000 keV for both detectors. The axes of the coincidence histogram were calibrated using a ^{152}Eu source. Software was written allowing the user to visually zoom in on coincident photo-peaks in either two or three dimensions, and select areas for background subtraction. The [136-264] keV ^{75}Se peak and [264-136] keV sister-peak volumes were found by summing the number of counts contained in the coincident histogram in a square centered on the peak centroid with sides of lengths ±1.5 FWHM for both detectors. Background estimation regions were selected to avoid any nearby Compton ridges.

Drying factors and dead-time correction

Prior to counting the primary reference materials, separate one gram fly ash and bituminous coal samples were dried for two hours at 105 °C in a DX-58 American Scientific Products drying oven. Typical diet, bovine liver, and oyster tissue samples were dried at room temperature for 24 hours at an absolute pressure of -60 kPa gauge pressure in a Fisher 281 vacuum oven. Separate samples were used due to the potential vaporization of Se. Samples were weighed before and after counting to obtain drying factors.

The dead-time and random-summing correction factors DTDT were measured via the use of an Ortec 480 pulser operating at 60 Hz. Pulser output was connected in parallel to the test-inputs of both detectors as depicted in Figure 8.

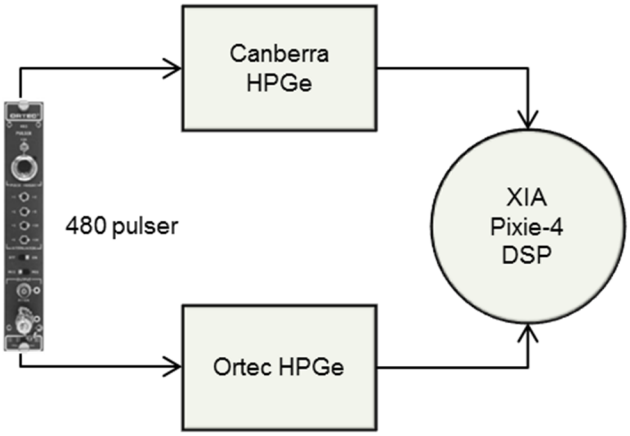

Figure 8: Block diagram for 480 pulser input

The pulses were attenuated to obtain signal peaks at interference-free spectral regions at 435 keV in the Canberra detector and at 360 keV in the Ortec detector. The bifurcated pulses were observed to arrive in coincidence within the time resolution of 13 ns of the DSP, and consequentially within the 500 ns timing window. Therefore, the pulses generated a coincidence peak at [435-360] in the coincidence histogram. Ten-minute pulse counts were taken before and after each 24-hour count with the sample present. The pulser was not operated during the 24-hour sample counts in order to prevent any interference with ^{75}Se peak shapes. A representative ten-minute pulser peak is depicted in Figure 9 counted with a fly ash reference material. White space depicts cells with zero counts.

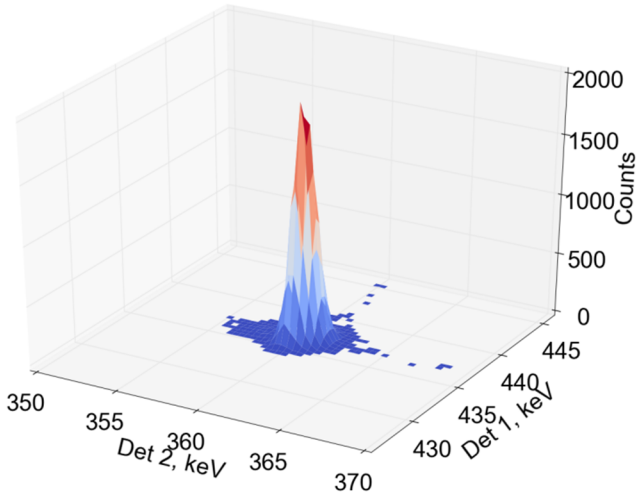

Figure 9: 10-minute pulser peak at [436-360] keV counted with fly ash

Net pulser-peak volume uncertainty was obtained by taking the standard deviation of a set of ten pulser counts with the fly ash reference material with the highest incident count rate on both detectors of about 8,500 counts per second. The % standard deviation of net pulser-volume was found to be 0.16%. The dead times before and after the counting period tt, D_0D_0 and D_fD_f, were calculated by dividing the expected counts by the measured net counts CC according to Eq. 20.

$$DT_i = \frac{60t_i}{C_i}, \qquad \sigma_{DT_i} = \frac{60t}{C_i^2}\sigma_{C_i} \tag{20}$$

The average dead-time over the 24 hour counting period t is given by Eq. 21 which assumes an exponential dead-time response function with time constant τ.

$$DT_{ave} = \frac{(DT)_0 T_0}{\tau t}(1 - e^{-\tau t}) \tag{21}$$

The time constant τ is calculated via Eq. 22.

$$\tau = \frac{\ln(DT_0) - \ln(DT_f)}{t} \tag{22}$$

The uncertanties of τ and $DT_{ave}DT_{ave}$ are calculated via the standard partial derivates methodology and are given in Eqs. 23 and 24.

$$\sigma_\tau = \frac{1}{t}\sqrt{\left(\frac{\sigma_{DT_0}}{DT_0}\right)^2 + \left(\frac{\sigma_{DT_f}}{DT_f}\right)^2} \tag{23}$$

$$\sigma_{DT_{ave}} = DT_{ave}\sqrt{\left(\frac{\sigma_{DT_0}}{DT_0}\right)^2 + \left(\frac{\sigma_\tau}{\tau}\right)^2 + \left(\frac{te^{-\tau t}\sigma_\tau}{1 - e^{-\tau t}}\right)^2} \tag{24}$$

This exponential fit was applied to dead-times above 2%. For low-activity samples, dead-times were calculated by simply averaging the dead-times associated with the before and after pulser counts. Table 1 depicts the drying and dead-time factors.

Table 1: Dead-time and drying factors[1]

Sample	DT factor	Drying factor
Se standard	1.001(1)	
Oyster tissue (1566a)	1.020(1)	1.010(2)
Bovine liver (1577b)	1.017(1)	1.024(4)
Typical diet (1548a)	1.006(1)	1.15(3)
Fly ash (1633a)	1.188(3)	1.0012(2)
Fly ash (1633b)	1.181(14)	1.0034(7)
Bit. coal (1632d)	1.019(9)	1.016(3)

Random-coincidence correction

The number of random-coincidences within the ^{75}Se [136-264] coincident photo-peaks was determined via post-processing of the list-mode data. A second 8192x8192 histogram was created from the list mode data from each count storing random-coincidences. This was achieved by only storing counts in the histogram where the Canberra detector registered energy within a time interval 50±0.5 μs ahead of the Ortec

[1] All uncertainties in parentheses are one-sigma

detector. After 50μs, no true coincidences with negligible energy-level half-lives would be expected. The random-coincidence photo-peaks were plotted from the time-delayed histogram in the same manner as in the non-delayed histogram. Figure 10 depicts two-dimensional images of random-coincidence histogram slices spanning the ^{46}Sc [1121-889] keV and ^{75}Se [136-264] keV photo-peak regions. White space depicts cells with zero counts. ^{46}Sc accounts for a significant amount of total activated fly-ash activity. This leads to a significant amount of random-coincidences between the primary 1121 and 889 keV ^{46}Sc γ-rays. However, ^{75}Se does not significantly contribute to total sample count-rate. Therefore, there exists no measurable amount of random-coincidences between the ^{75}Se 136 and 264 keV γ-rays in Figure 10. This is a strong quality assurance check that the measurement of the intensity of the non-delayed ^{75}Se [136-264] keV coincidences will not lead to an over-estimation of Se concentration due to the presence of random-coincidence counts. If ^{46}Sc concentration was being measured, then the number of random-coincidence [1121-889] keV counts would have to be subtracted from the total number of coincidences determined from the non-delayed histogram.

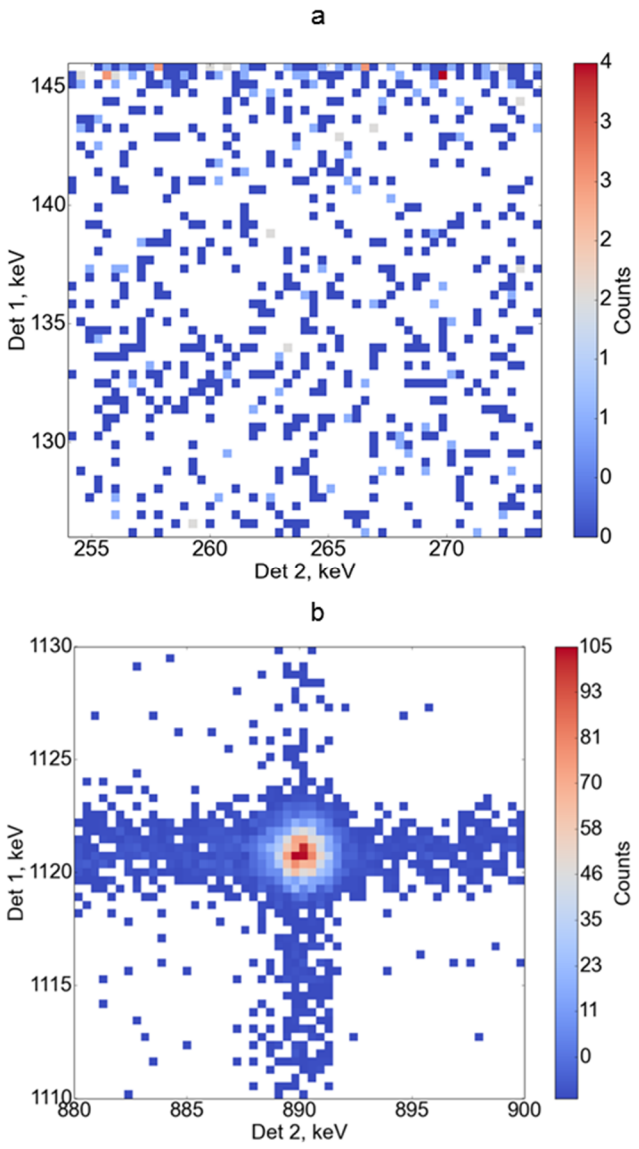

Figure 10: Random-coincidence histogram slices spanning the ^{75}Se [136-264] keV (a) and ^{46}Sc [1121-889] keV (b) photo-peak regions

After determining [136-264] keV coincidence-peak areas, calculating dead-time and drying correction factors, and verifying that no significant amounts of random-coincidences were present, reference material concentrations were calculated via the

NAA comparator method. The same procedure was applied to the [264-136] keV ^{75}Se coincidence sister-peak. The final Se concentration was determined by taking a weighted-average of the [136-264] and [264-136] keV peak volumes which each had a one-sigma uncertainty.

Results and discussion

Figure 11 depicts the ^{75}Se [136-264] keV photo-peak region for one of the fly-ash reference materials. White space depicts histogram cells with four or less counts for visualization purposes. One spectral phenomenon is a Compton ridge-line associated with ^{181}Hf 133 keV γ-rays in coincidence with Compton scattering events from the coincident 346 and 482 keV γ-rays. The ridge is just outside of 1.5×FWHM of detector one and no subtraction was needed. The left tail on detector two is also apparent. The background region was chosen to avoid the left tail and also any Compton ridge phenomena.

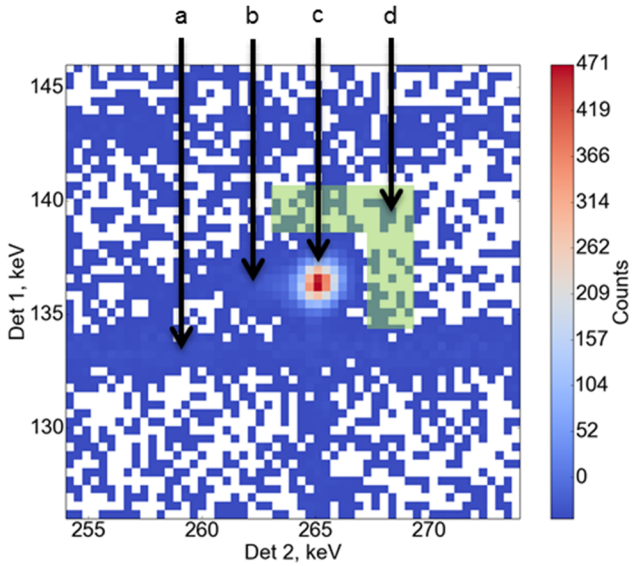

Figure 11: Fly ash ^{75}Se [136-264] keV photo-peak (c), ridge from ^{181}Hf 133 keV γ-ray in coincidence with ^{181}Hf Compton events (a), Canberra detector left-tail (b), background estimation region (d)

The peak-to-background ratio, here defined as the ratio of net peak intensity to background intensity, for the 264 keV ^{75}Se photo-peak taken from the standard singles spectrum is 0.129(1), without any deconvolution of interferences. The peak-to background ratio of the coincident ^{75}Se [136-264] keV photo-peak depicted in Figure 12 is 12.5(5). This represents a substantial improvement in signal-to-noise ratio over the singles spectrum.

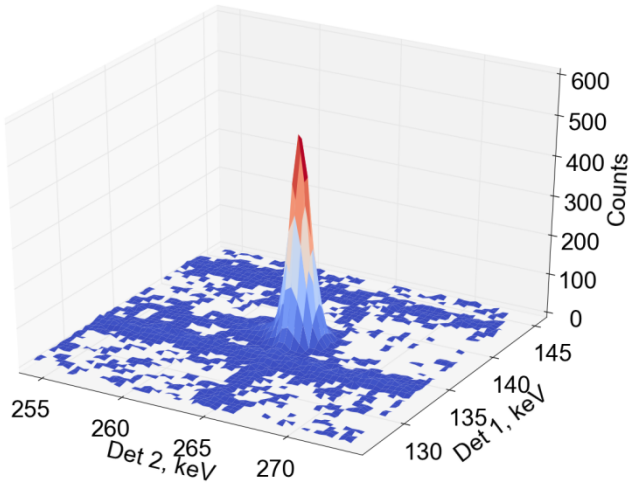

Figure 12: [136-264] keV 75Se coincidences in fly-ash

One sample of each of the six NIST reference materials was analyzed. The agreement within uncertainty of the NIST referenced and measured concentrations given in Table 2 suggests the presented methodology has the potential to accurately determine Se concentrations in samples with moderate activities and interferences.

Table 2: Se concentrations of six NIST reference materials

Sample	Reference conc. [μg/g]	Measured conc. [μg/g][2]	MDA [μg/g] [34]
Oyster tiss. [1566a]	2.21(24)	2.14(9)	0.76
Bov. Liver [1577b]	0.73(6)	0.69(4)	0.48
Typical diet [1548a]	0.25(3)	0.24(2)	0.42
Fly ash [1633a]	10.3(6)	10.10(15)	0.56
Fly Ash [1633b]	10.26(17)	10.02(17)	0.55
Bit. Coal [1632d]	1.29(3)	1.31(4)	0.30

Conclusions

Selenium concentrations were accurately determined in fly ash, coal, and biological samples via the application of γ-γ coincidence techniques. Determining coincident peak volumes in the two-dimensional histogram eliminated the ^{181}Hf and ^{182}Ta interferences. A straightforward methodology has been presented to setup a coincidence system capable of accurately determining the concentrations of isotopes with coincident γ-rays in moderate dead-time spectra. Many of the techniques presented in this chapter

[2] Uncertainties are given in parentheses. Reference concentration uncertainties reported by NIST span the uncertainty range from multiple methodologies. Measured concentration uncertainties are reported as one-sigma.

will be applied to the analysis of fission-product spectra of similar complexity in chapter 4.

Chapter 3: Dead-time analysis

Abstract

This chapter outlines a methodology to correct for dead-time in a coincidence system specific to the XIA digital signal processor (DSP). The method is experimentally verified by the counting of an activated manganese sample. Further, the chapter explores the capability of a coincidence system to suppress natural background without the aid of a dense metal shield.

Introduction

This chapter draws heavily from the XIA PIXIE-4 manual [35]. Assuming randomly occuring pulses governed by Poisson statistics, HPGe detectors suffer from paralyzable dead-time [36]. The relationship between output count rate (OCR) and input count rate (ICR) is governed by the equation

$$OCR = ICR * e^{-2\tau * ICR} \tag{25}$$

Where ττ is the pile-up inspection time approximately equal to the energy-filter shaping time. There exists a factor of two in Eq. 25 because if a pulse A occurs at time tt, it is invalidated if a second pulse either arrives in a time period t-τt-τ or t + τt + τ. Now, say that a coincidence occurs where energy is deposited in both detectors at time tt. This

coincident event will be invalidated if a tertiary particle deposits energy in the first detector within a time period $t\text{-}\tau_1 t\text{-}\tau_1$ or $t + \tau_1 t + \tau_1$, where $\tau_1\tau_1$ is the pile-up inspection time for the first detector. The coincident event will also be invalidated if a tertiary particle deposits energy in the second detector within a time period $t\text{-}\tau_2 t\text{-}\tau_2$ or $t + \tau_2 t + \tau_2$, where $\tau_2\tau_2$ is the pile-up inspection time for the second detector. Therefore, the probability of the coincident event being validated is given by

$$\frac{OCR_{coincidence}}{ICR_{coincidence}} = \left(e^{-2\tau_1 * ICR_1}\right) * \left(e_2^{-2\tau_2 * ICR_2}\right) = e^{-2(\tau_1 ICR_1 + \tau_2 ICR_2)} \qquad (26)$$

All of the experiments depicted in this thesis employ asymetric detectors with different efficiency curves and different shaping factors optimized for resolution. Therefore, it is important to maintain the generalization of Eq. 26 and not assume a universal shaping factor and input count rate. There is also a small correlation between the probability of tertiary particles interacting with both detectors due to true coincidences being emitted or by coincident Compton events. However, for the detection system considered in this Chapter, even with a pure ^{60}Co source, only about 0.7% of the events stored by the DSP are true coincidences between the 1173.2 and 1332.5 keV γ-rays. Therefore, this correlation will be neglected in this analysis and the following chapters.

In the PIXIE-4 DSP, the pile-up inspection time is roughly equal to the energy filter rise time and flatop time, plus a few 13.3 ns clock cycles. The shaping factors can be easily computed from the meta-data supplied for each count in a text file. The meta-

data text file (.ifm) includes the count-rate of the number of fast-filter triggers for each detector which either pass or fail pile-up inspection if they occur within a time interval ± ττ of a second pulse. This fast trigger count-rate can be taken as an approximation to the input count rate. Further, PIXIE-4 reports the output count rate for each detector. Using these two reported values for the input and output count rates, ττ can be calculated for each detector ii by

$$\tau_i = -\ln\left(\frac{OCR_i}{ICR_i}\right)/2ICR_i \tag{27}$$

Once the pile-up inspection times are computed, the total coincidence dead time can be determined by Eq. 26.

One slight complication to this procedure is the additional dead time when the DSP is busy conducting auxilliary tasks such as writing buffer data to the final output file. PIXIE-4 reports the total time, which is an attempt to measure the laboratory time from the start to the end of count. PIXIE-4 also reports the run time, which omits time lost to auxilliary tasks. Therefore, a methodology to determine coincidence count rates corrected for dead time is to take the net counts underneath a peak, divide by the run time, and then multiply by the dead time correction factor depicted in Eq. 26.

Experimental and results

A 25% relative efficient stationary Canberra coaxial HPGe model GC2518 S/N 9997089 was combined with a 15% relative efficient Canberra portable coaxial HPGe model GC1519 S/N 09037704 in a coincidence system without any lead shielding depicted in Figure 13. This detection system will be also be utilized in chapters 4 and 5.

In order to demonstrate the lack of a need for a dense metal shield if utilizing the coincidence spectrum, a 24 hour background count was taken.

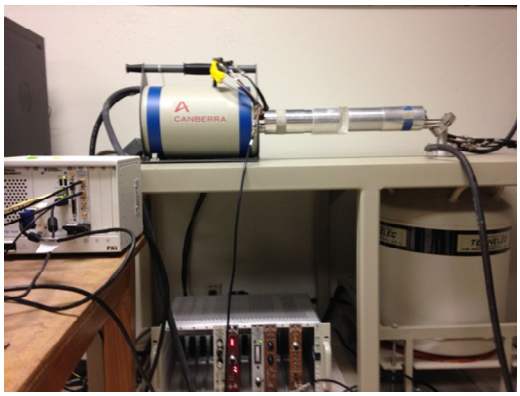

Figure 13: Detection system used in chapters 3, 4, and 5

Figure 14 represents the coincident spectrum or most intense background region spanning 0 to 250 keV for both detectors. Note that the number of counts in each bin never exceeds more than a few counts, and the majority of the coincident spectrum contains white space, representing zero counts. This can be contrasted with Figure 15 which represents

the one-detector background spectrum with relatively high background levels, especially below 250 keV.

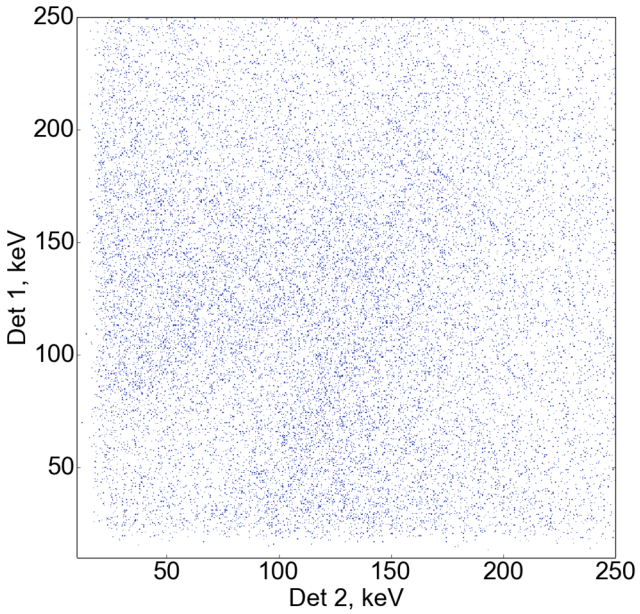

Figure 14: Coincident 24hr background spectrum[3];

[3] white space depicts channels with zero counts; blue channels contain one count

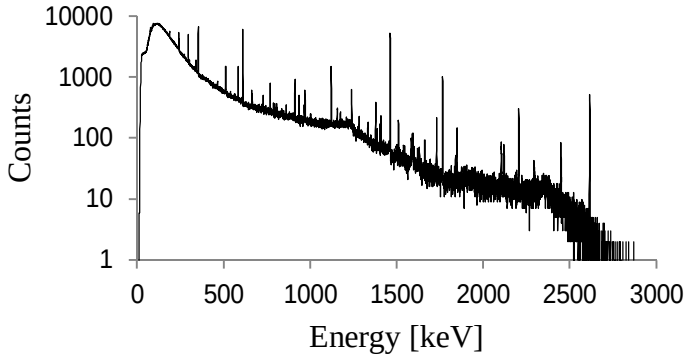

Figure 15: Single detector 24hr background spectrum

In order to test the validity of Eq. 26, a manganese sample was irradiated for two minutes at full reactor power in order to obtain sufficient activity of ^{56}Mn to produce an initial system input count rate of 300,000 counts per second. 20 minute counts were taken over the course of ten half-lives ($t_{\frac{1}{2}} = 2.58 t_{\frac{1}{2}} = 2.58$ hrs). The number of [847 1810] keV coincidences were recorded in each spectrum and corrected for random coincidences. Coincidence input count rates were determined by using the final Mn count with effectively zero dead time as a reference point. From this final input count rate, input count rates for all of the other 20 minute counts were determined by correcting for radioactive decay. Finally, Eq. 26 was used to predict the number of output coincidences, given the information contained in the meta-data. Observed and predicted coincidence count rates were plotted together as functions of coincidence input count rate in Figure 16. The dead-time model accurately predicted output count rates up to about 45,000 counts per second. This point occurs at the dead time 'hump' where counting throughput

is optimized. After this point, the dead time model begins to break down. It is hypothesized that this is the case due to the predominance of random summing [36].

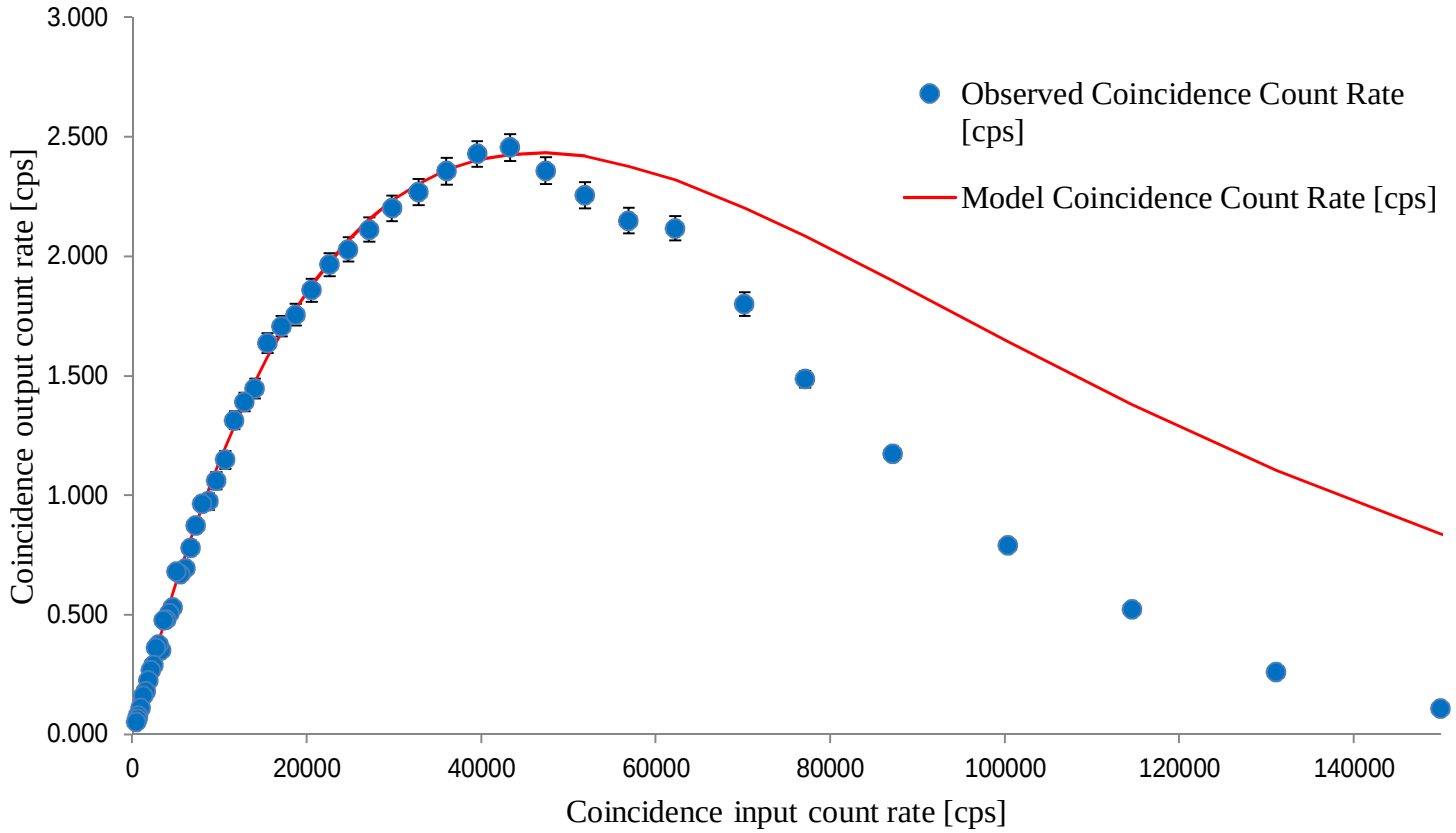

Figure 16: Dead time analysis using activated manganese

Conclusions

Very low natural background levels taken with the HPGe coincidence system indicates the potential lack of need for dense metal shielding. Further, a basic dead time model was developed which utilizes the meta data supplied by the DSP. The dead time model proved valid up to about the maximum detection system throughput. It is hypothesized that at higher count rates, the model begins to break down due to the predominance of random summing. While this method is straightforward to calculate, it is not as accurate as the pulser method detailed in chapter 2 which will take into account random summing as well as dead time.

Chapter 4: Fission product analysis

Abstract

The fission product γ-spectrum consists of a large number of interfering signatures amidst a high Compton-continuum from such intense γ emitting isotopes as ^{137}Cs. Coincidence counting techniques have the potential to eliminate these high background situations and achieve higher detection limits and better relative uncertainties for multiple low-level isotopes. A methodology is developed to quantitatively determine fission isotope concentrations using γ-γ coincidence counting. A fission-product spectrum is generated via irradiating a depleted U solution in the TRIGA Mark II reactor at the University of Texas at Austin and counted in a γ-γ coincidence system. A Scale 6.1.3 activation model of the reactor is developed to simulate the isotopic vector of the sample to aid the spectrosopist in peak identification in the complex coincidence spectrum. ^{140}La activities were determined from the coincidence peak-volumes and coincidence intensities generated with MCNP modelling. Exerimental and simulated ^{140}La activities agree within . The methodology, in addition to determining fission-product activities, has the capability to quantitatively determine which fission-products may benefit from γ-γ coincidence counting techniques.

Introduction

Many multi-detector system methodologies have been explored to determine fission-products. A β-γ coincidence system was utilized to determine ultralow activities of ^{131m}Xe, ^{133m}Xe, ^{133}Xe, and ^{135}Xe isotopes [37]. This work was added to by utilizing a 24-element Si PIN diode detector to determine Xe ratios not only by β-γ, but also by gating off of conversion electrons and x-rays [38]. This work was furthered this work by developing a methodology to determine β-γ coincidence efficiencies for Xe determination using a GEANT4 model [39].

Compton suppression has also been explored as a method to lower background levels and decrease detection limits in fission product spectra using a 52% efficient coaxial HPGe surrounded by a 2 inch NaI(Tl) active shield [40]. It was demonstrated that Compton suppression lowered the detection limits by a factor of three for ^{137}Cs and by a factor of two for ^{54}Mn for low-activity swipes. Recently HPGe and $LaBr_3$ Compton suppression systems were used to analyze fission product spectra in spent fuel samples [41]. Multiple spectral features were able to be resolved from one-year cooled spent fuel including the 48 and 427 keV peaks from ^{125}Se, the 835 keV peak from ^{54}Mn, and the 1040 keV peak from ^{134}Cs. The detector system was further modelled in GEANT4. However, the model did not have the capability to simulate correlated photon decay. Rather, the model was built in order to simulate a complete spent fuel sample at once.

Therefore, photopeak losses due to cascade emissions from isotopes with complex decay schemes such as ^{154}Eu were not taken into account.

There have also been explorations into the capability of γ-γ coincidence to determine spent fuel composition. A xenon-doped liquefied argon (Lar(Xe)) scintillation coincidence system was developed for the detection of the prompt γ emissions of illicit nuclear materials generated via a d-d neutron generator [42]. Recently, a GEANT4 model was developed in order to determine the coincidence efficiencies for fission products generated via irradiating uranium foils [6]. However, to the best of knowledge of this thesis, no definitive study has been conducted which determines the quantitative improvement to relative uncertainties and detection limits γ-γ-coincidence may give to fission products. This thesis focuses on developing the expertise and methodology in order to develop such a list. While the methodology is validated by only one isotope, ^{140}La, is is planned for future work that the tools developed in this thesis will be used to generate a definitive list the quantitative benefit of γ-γ-coincidence to approximately 183 fission products with half-lives greater than two days including progeny in secular equilibrium.

The Monte Carlo tool used in this thesis to generate the correlated coincidence intensities is MCNPX-PoliMi v2.0. Polimi is an extension to MCNP originally developed as a modification to MCNP4C to simulate correlated counts in scintillation detectors of fast neutrons and γ-rays [43]. In relation to radioactive decay, PoliMi parses the ENDSF

files to determine the multiple photons emitted for each decay. Then, the multiple particles are tracked for the particular history and the energy deposition in whichever cells are tallied can be tracked.

PoliMi has been used for a variety of non-proliferation applications. [44] used PoliMi to model neutron and gamma-ray responses in a six liquid scintillator system from plutonium-oxide samples and a ^{252}Cf source. PoliMi was used to investigate perturbations in various photoneutron reactions for active photon interrogation purposes [45]. Another study used PoliMi to investigate a neutron detector response to Pu spheres [46]. The work focused on determining the multiplication factor $k_{eff}k_{eff}$ from the detector response.

When modelling γ detection systems via Monte Carlo means, one of the most critical factors to consider is obtaining the correct detector dead-layer. The surface dead layer may vary slowly with time due to the formation of surface channels [47]. This is especially the case for detectors which sit at room temperatures for extended periods of time, as is the case for the detectors in utilized in this thesis chapter. Another study conducted a parameter sweep of the dead layer thickness and other geometric parameters of a GEANT 4 model to determine the dead layer of an HPGe detector from the response from a point source [48]. The dead-layer was determined to be an increasing function with crystal depth, at all points greater than that stated on the specification sheet. A more recent study found a very large discrepency between the specified dead layer thickness of 0.4μm and the experimentally determined dead layer thickness of 7.5μm in a low-energy

HPGe [49]. A further study found an increase in dead layer thickness from 1.15 to 1.46 mm over the course of four years [50]. A three-fold increase in thickness from 0.35 to 1.16 mm over a period of nine years [51]. A final study found a dead layer thickness of 1.5 mm which was twice the certified value [52].

Experimental

Sample irradiation and reactor model

A one mL Inorganic Ventures 10,270(46) μg/mL uranium standard was irradiated in the TRIGA Mark II reactor. Sample uranium isotopic distribution was 99.7(1) atom % ^{238}U and 0.29(5) atom % ^{235}U. The greatest source of uncertainty in this experiment is the high 17% uncertainty associated with the ^{235}U sample atomic abundance. The sample was irradiated for 1.5 hours at a power level of 950 kW. The average neutron flux at the sample at this power was modelled to be 6.5×10^{12} cm^{-2} s^{-1} with a thermal flux above a 0.625 eV cutoff of 2.9×10^{12} cm^{-2} s^{-1} . The sample was automatically revolved around the reactor core in order to achieve a uniform flux distribution. The sample was then removed from the reactor and decayed in storage for 63 days prior to counting.

In order to simulate the activation process and develop an independent ^{140}La activity for quality assurance, a Scale version 6.1.3 [53] reactor model used for reactor safety analysis at NETL was modified to include the uranium standard in the approximate activation position. The V7-238 cross-sectional library was used to generate 238 initial

neutron energy groups. It was felt that due to the large fast component to the neutron flux in the TRIGA reactor coupled with the high ^{238}U abundance relative to the fissile ^{235}U content in the sample necessitated the use of this activation model to take into account fast fission. A cut-out view of the model is depicted in Figure 17.

The SCALE model was then set to deplete the sample using the reactor power and time specifications equal to the actual physical reactor run. A comprehensive fission product list was taken from the Scale manual [53]. From this list, the activities of 183 fission products at the end of the reactor run and 63-day decay period with half-lives greater than two days including decay-products were set to be reported by ORIGEN-ARP. During a few trial runs, the position of the control rods was modified to obtain a $0.995 < k_{eff} < 1.0050.995 < k_{eff} < 1.005$ in order to properly simulate the flux profile. One million neutron generations was used in order to obtain as accurate a number as possible in the course of a day while running on a quad-core processor.

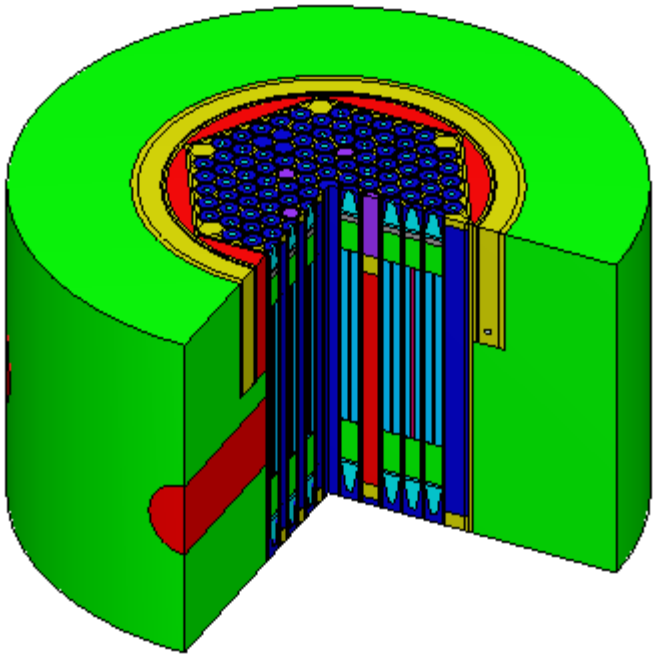

Figure 17: Scale 6.1.3 model of TRIGA Mark II reactor at UT Austin[4]

In order to simulate the circular motion of the source during the reactor run, eight identical uranium samples were placed equidistant from the reactor center-line along the travel path. Figure 18 depicts a reactor model top-view showing the eight sample positions. After completion of the model run, the generated ^{140}La and ^{140}Ba activites were both divided by eight.

[4] Initial model built by Mike Whaley, Associate Director at NETL

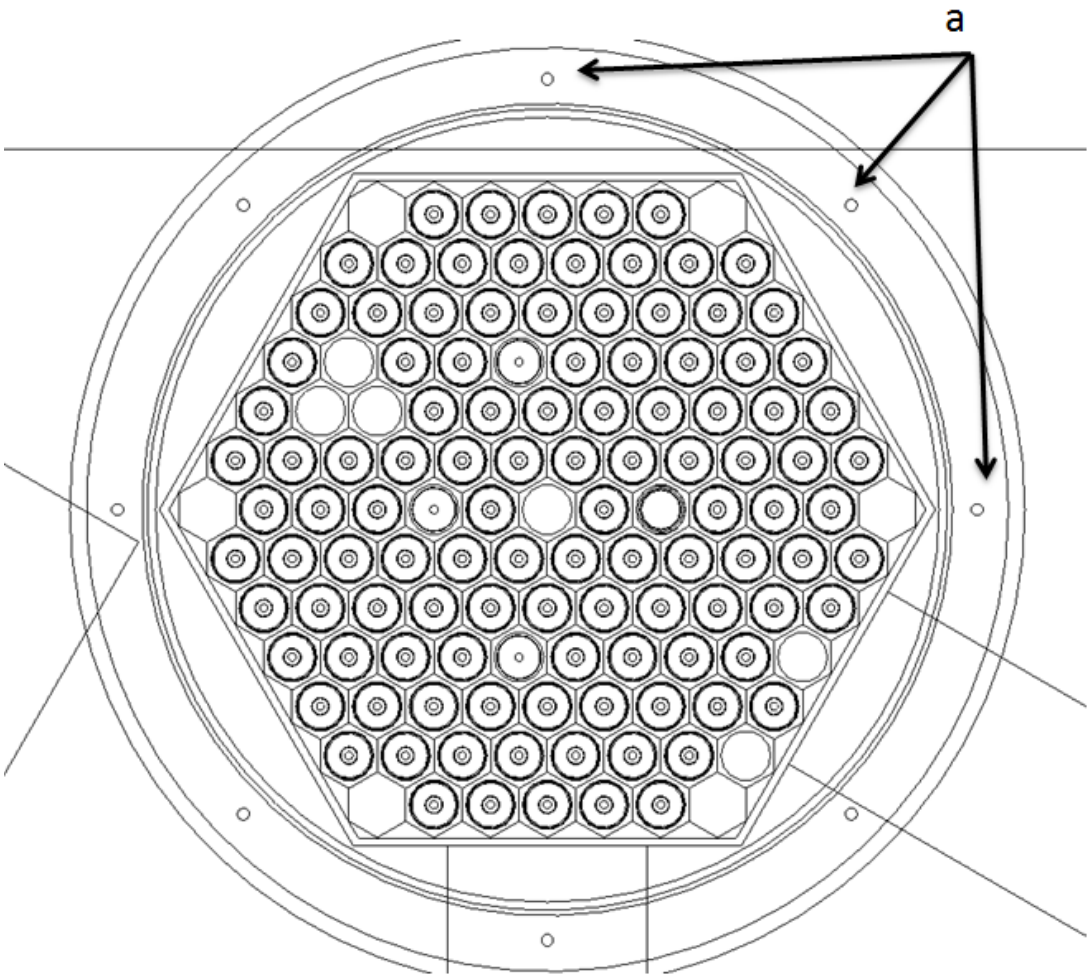

Figure 18: Top-view of reactor model; (a) 8 cylindrical uranium samples to simulate revolution during activation

A set of eight separate 200,000 neutron generation reactor runs were conducted with only one sample at each of the eight positions in order to determine the neutron flux variability as a function of position. Table 3 depicts the results of the eight reactor runs. The ^{140}La activity population standard deviation of the eight runs at different positions was calculated to be 6.7%.

Table 3: Variability of ^{140}La production as of function of reactor position

X coordinate [cm]	Y coordinate [cm]	^{140}La activity [Bq]
-23.3	-23.3	712
23.3	-23.3	601
-23	23	750
23	23	725
0	33	728
0	-33	739
33	0	763
-33	0	689

The reactor fuel and fuel cladding temperatures were set at 600 K. A more accurate model would take into account the variability of fuel temperature as a function of position. In future work, the reactor fuel peaking-factors will be calculated to determine the fuel-rod temperature distribution. In this thesis, a simple procedure was conducted to determine the uncertainty on ^{140}La and ^{140}Ba SCALE model activities due to variability in fuel temperature. A separate 300,000 neutron generation reactor-run was conducted with the fuel temperature set at 700 K. A 1.8% difference was found between the 600 K run and the 700 K run.

The primary source of uncertainty in the SCALE model generated activities is the uncertainty in the ^{235}U concentration in the 0.29(5) atom % ^{235}U standard. A separate 300,000 neutron generation reactor-run was conducted with a 0.34 atom % ^{235}U content. A 21% difference was found between the 0.29 and 0.34 atom % ^{235}U runs. The temperature and U content uncertainties were added in quadrature to get the final SCALE reactor % uncertainty of 21.1%. The high uncertainty associated with ^{235}U content

dominates the uncertainty of the SCALE model, fundamentally limiting the assessement of model precision. In future work, it is planned to irradiate enriched uranium foils to better assess model fidelity.

The SCALE model calculated ^{140}La and ^{140}Ba activities at the end of the 63 day decay period. At this point, ^{140}La was not yet in equilibrium with ^{140}Ba. Further, with ^{140}La and ^{140}Ba half-lives of 1.7 and 12.8 days, respectively, both will decay considerably during the counting duration. ^{140}La activity during the counting duration is taken from [54] as

$$\alpha_{La} = \alpha_{La}(t = 0)e^{-\lambda_{Ba}t} + \frac{\alpha_{Ba}(t = 0)\lambda_{La}}{\lambda_{La} - \lambda_{Ba}}(e^{-\lambda_{Ba}t} - e^{-\lambda_{La}t}) \tag{23}$$

where $\alpha_{La}(t = 0)\alpha_{La}(t = 0)$ and $\alpha_{Ba}(t = 0)\alpha_{Ba}(t = 0)$ are the initial ^{140}La and ^{140}Ba consentrations, respectively at the start of the counting period; $\lambda_{Ba}\lambda_{Ba}$ and $\lambda_{La}\lambda_{La}$ are decay constants; and ^{140}Ba activity $\alpha_{Ba}\alpha_{Ba}$ is given by

$$\alpha_{Ba} = \alpha_{Ba}(t = 0)e^{-\lambda_{Ba}t} \tag{24}$$

For comparison to the experimental results, average ^{140}La activity during the course of the counting duration $t_c t_c$ was calculated by

$$\overline{\alpha_{La}} = \frac{1}{t_c}\int_0^{t_c} dt\alpha_{La} \tag{25}$$

PoliMi model

Detection system geometry was modelled with information from the specification sheets. Modelling geometry took into account:

1. Aluminum housing
2. Aluminum crystal holder
3. Outer electrode (outer dead layer) on crystal top and sides
4. 1/3 mil mylar film in the IR window
5. 4 mil Kapton layor in IR window
6. Aluminum coating on IR window
7. Copper core signal contact
8. Teflon insulator
9. Steel table underneeth detectors
10. Plastic sample-holder

An image of the MCNP geometry is depicted in Figure 19.

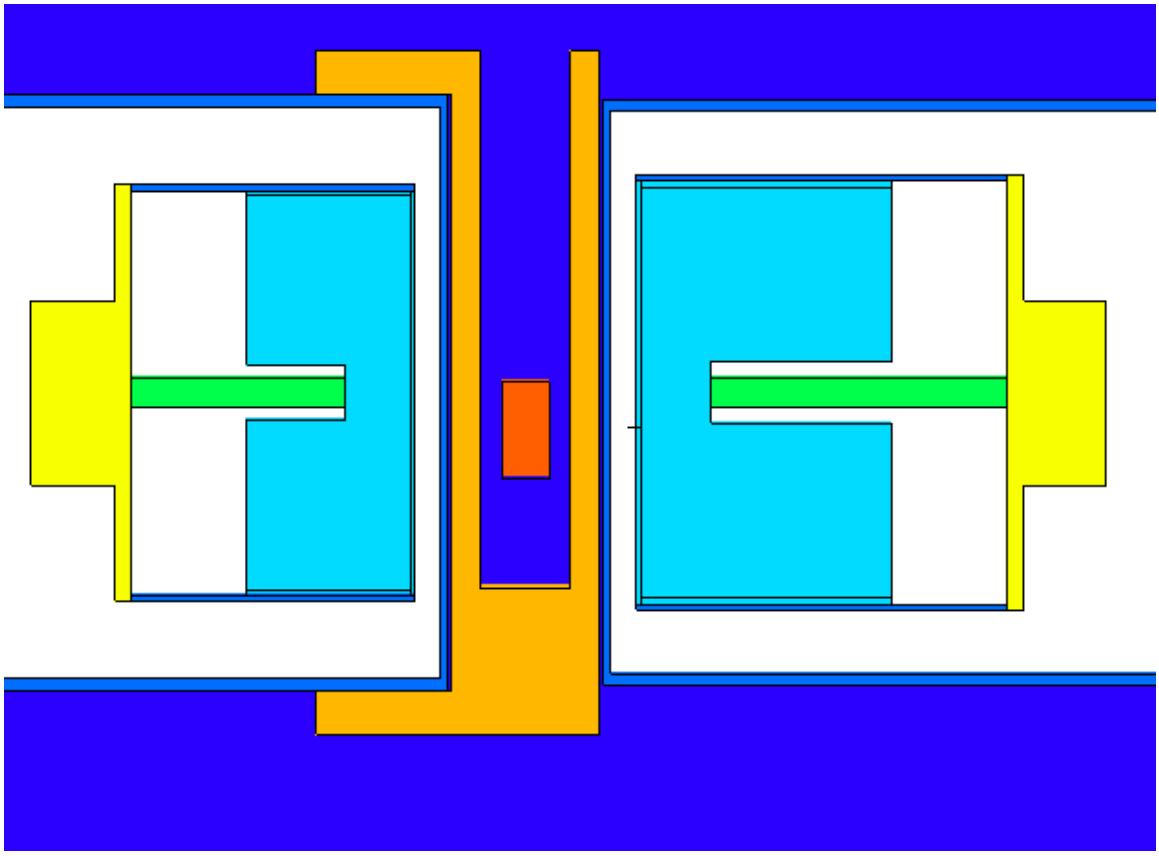

Figure 19: Geometry of MCNP coincidence system model

In order to develop a high-fidelity MCNP model, the correct dead-layer thicknesses for both detectors must be determined. This is especially important for the two detectors modelled. The right detector sat warm for several years before being integrated into the coincidence system, and the left portable detector has undergone multiple thermal cycles in addition long periods of sitting warm over its lifetime. To accomplish this task, a certified ^{137}Cs source was counted for ten minutes at the face of both detectors. A

spectrum from the right HPGe detector generated with the ^{137}Cs source is depicted in Figure 20.

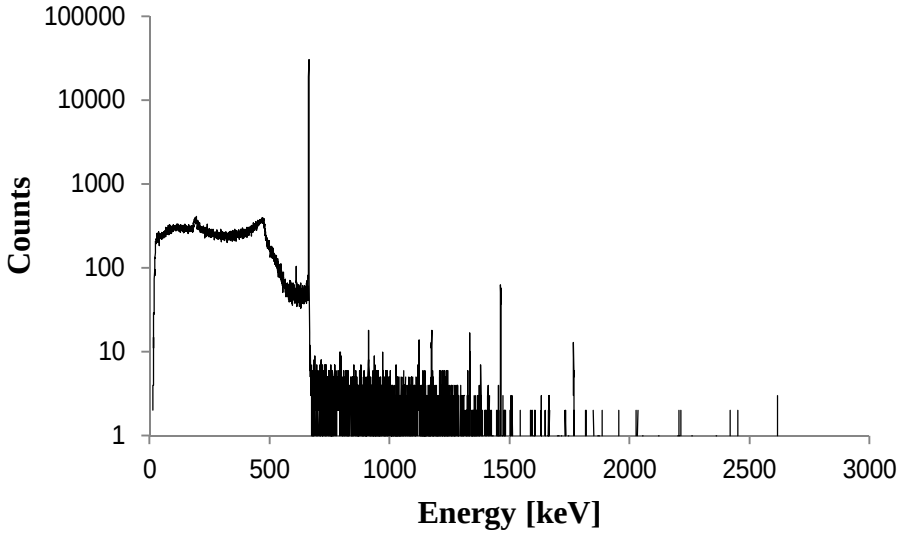

Figure 20: ^{137}Cs spectrum used to determine dead-layer thickness of left detector

A standard F8 tally was used to simulate the number of 662 keV ^{137}Cs counts deposited in each detector. In order to produce spectral resolution in the MCNP model, resolution curves were taken with a ^{152}Eu source for both detectors. A set of one-hundred million dissintegration MCNP runs were then generated with different dead layer thicknesses ranging from 0.1 to 2 mm. The experimental data, corrected for dead-time according to the methodology in Chapter 3, matched the MCNP data when the portable detector dead-layer thickness equalled 0.6 mm and the stationary detector dead-layer thickness equalled 1.1mm. The portable and stationary specification sheet thicknesses at the date of manufacture are 0.44 and 0.69 mm, respectively. This increase of thicknesses of 57% and

59% for the portable and stationary detectors, respectively, is consistent with previous reports in the literature [48,52,49,47,50,51]. Figure 21 depicts the results of the MCNP dead-layer thickness parameter sweep. In Figure 21, the 662 keV efficiency varies by as much as 50% for thicknesses between 0.1 and 2 mm. This demonstrates the necessity for obtaining accurate dead-layer thickness values for HPGe detectors.

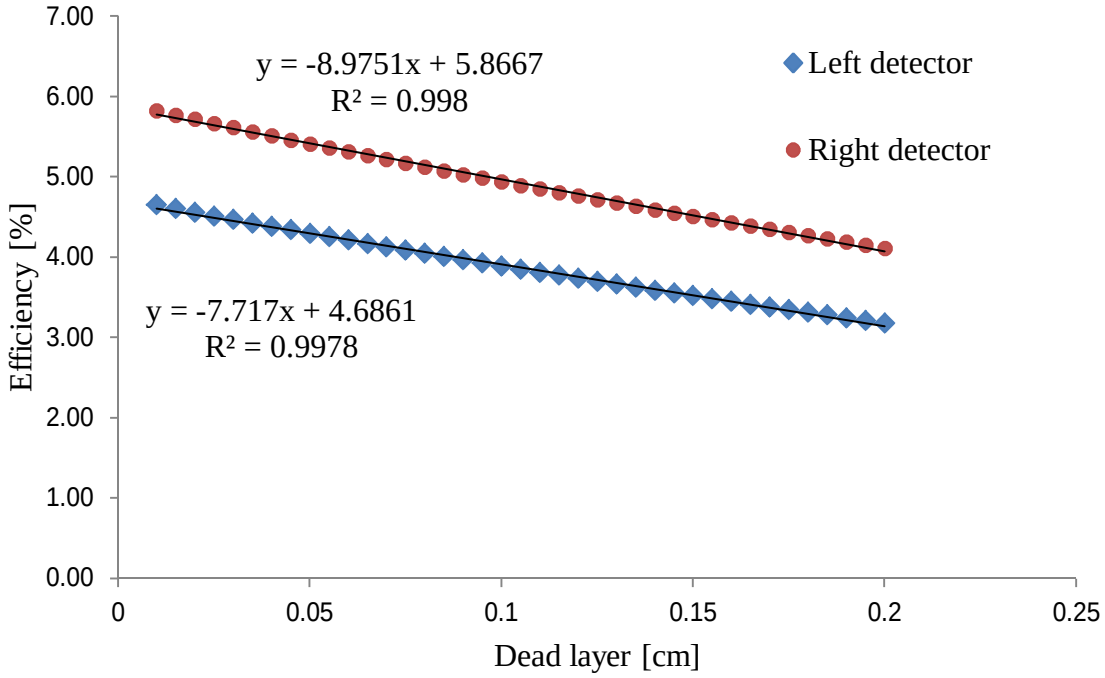

Figure 21: MCNP parameter sweep of dead layer thickness

The final MCNP input deck, optimized for dead-layer thickness, is depicted in Appendix A.

After developing a high-fidelity detector model, The aqueous uranium solution was filled with a distributed ^{140}La source using the PoliMi source definition. Ten million dissintegrations were then conducted and F8 talleys were placed on both Ge crystals. A separate coincidence matrix spanning 0 to 3000 keV on both axes was then generated containing the energy deposited in detector 1 and detector 2 during the same dissintegration. The top ten simulated coincidences were then taken from this matrix. For example, at [487 1596] keV, PoliMi generated 7,760 registered coincidences. The coincidence intensity for [487 1596] keV is then given as

$$I[487\ 1596] = \frac{7{,}760 counts}{10{,}000{,}000\ dis.} = \frac{7.60x10^{-5} counts}{dis.}. \quad (26)$$

Experimental data

The measured number of counts in the acquired coincidence spectrum for each of the top ten coincidences reported by the PoliMi model were then found via the procedures outlined in Chapter 2. Dead-time was determined to be 8% via the methodology outlined in Chapter 3. A draw-back of using PoliMi is that it does generate angular correlations between particles. Therefore, angular-correlations between the coincident γ-rays were generated post-processing. All angles were assumed to be 180°°. Angular correlations were calculated via Eqns. 11 and 13. This does not take into account angular correlations between tertiary particles depicted in Eq. 7. It also does not take into

account the variation of the angular correlation accross the solid angles subtending the source and detectors.

Results and discussion

Figure 22 and Figure 23 depict the [1596-328] and [1596-815] keV coincidences of ^{140}La . White space depicts cells with zero counts. As can be seen, background has been virtually eliminated except for the Compton ridges. Note that the reported coincidence efficiencies from PoliMi include counts underneath the coincidence photopeak from any Compton events occuring from other γ-rays associated with the decay path. Therefore, when computing background levels, the four 'flat' regions above and below the Compton ridges should be used. Therefore, the ridges should not be deconvoluted from the peak-volume. Rather, all counts within ± ± 1.5 FWHM of the centroid should be used for gross counts. Figure 22 and Figure 23 may be compared to Figure 24 which depicts the conventional, portable HPGe spectrum for the ^{140}La count. Comparing the coincident and conventional spectra demonstrate the significant decrease in background levels achieved by the coincidence system.

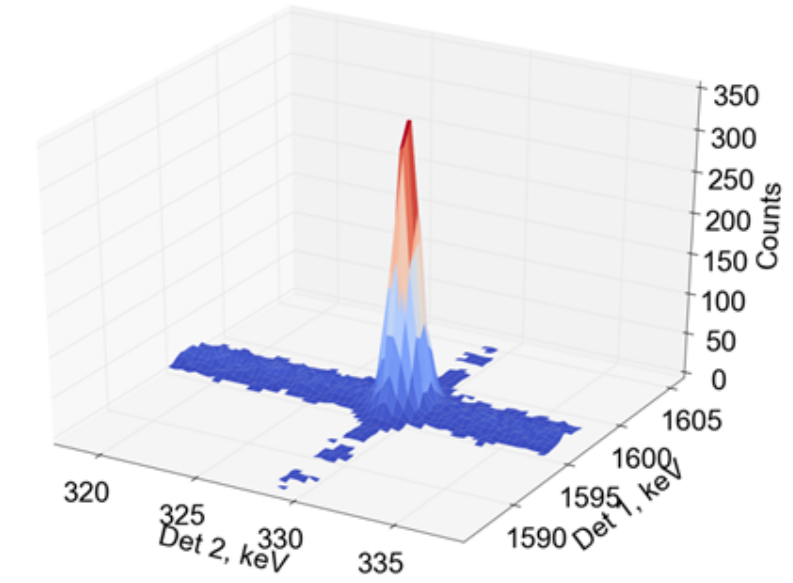

Figure 22: [1596-328] keV coincidence for ^{140}La.

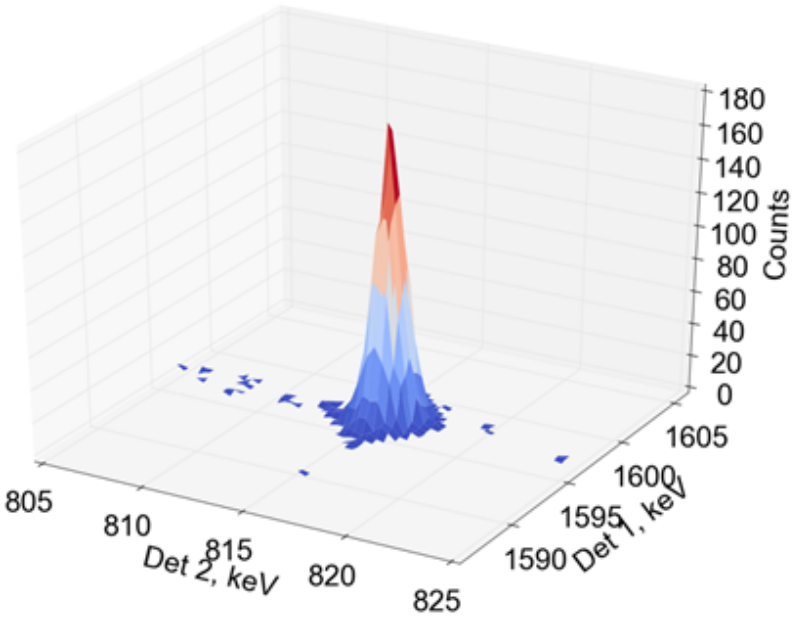

Figure 23: [1596-815] keV coincidence of ^{140}La

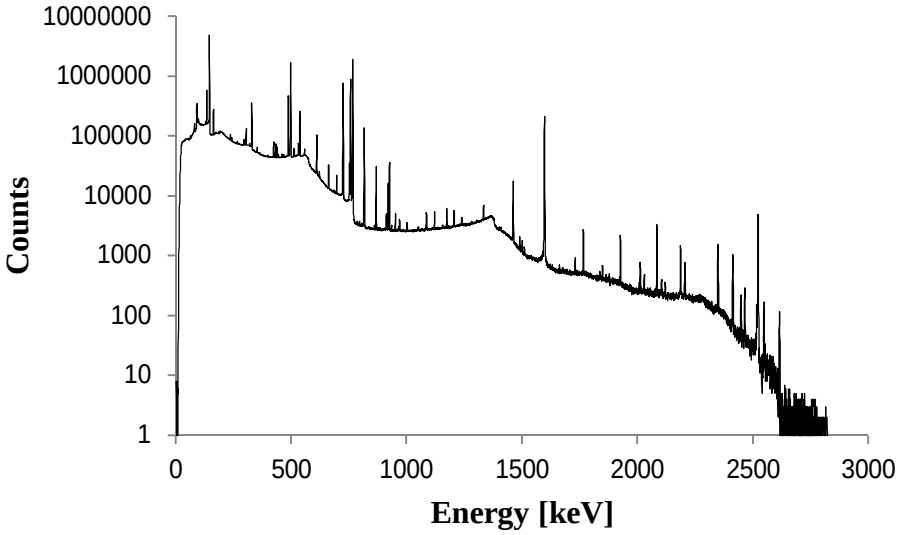

Figure 24: ^{140}La spectrum from a single HPGe

Table 4 depicts the average ^{140}La activites over the counting period generated from the SCALE model and experimental data. For the sister coincidences such as [487-328] and [328-487] keV, the coincidence efficiencies should not be identical since detectors with different efficiencies were employed. Note that for sisters with close energies, coincidence efficiencies are nearly identical. However, for sisters with significantly different energies such as [1596-487] and [487-1596] keV, the coincidence efficiencies differ significantly due to the detectors having different efficiency shapes.

Table 4: Results of SCALE and experimental ^{140}La average activities[5]

Coincidence [keV]	PoliMi efficiency [counts/diss.]	Experimental activity [Bq]	SCALE model activity [Bq]	SCALE/ Experimental
[487 328]	1.500E-04	625(63)	660(140)	1.03
[328 487]	1.460E-04	595(60)	660(140)	1.09
[1596 487]	8.710E-05	536(54)	660(140)	1.21
[487 1596]	7.760E-05	518(52)	660(140)	1.25
[1596 328]	5.556E-05	555(60)	660(140)	1.16
[328 1596]	4.690E-05	523(53)	660(140)	1.24
[1596 815]	3.320E-05	541(55)	660(140)	1.20
[815 1596]	2.980E-05	560(57)	660(140)	1.16
[432 487]	1.620E-05	700(71)	660(140)	0.92
[487 432]	1.600E-05	699(71)	660(140)	0.93
Ave. Experimental activity [Bq]:		585(65)		
Scale Model activity [Bq]:		657(138)		
Percent difference:		11%		

Experimental ^{140}La activities for sister coincidences are nearly identical. However, there are significant differences between experimental activities between separate coincidence pairs. The span is from 518(52) Bq for [487 1596] keV to 700(71) Bq for [432 487] keV. This indicates a fundamental issue with deriving coincidence efficiencies via modelling: the results will only be as good as the nuclear data. Whereas data is generally good for γ intensities for well-studied isotopes, tertiary particle information such as x-ray intensities and fluorescenses which all contribute to total

[5] All reported uncertainties in parentheses are one-sigma

coincidence intensities may not be so accurate [4]. A further contribution to this spread in ^{140}La activity for the various coincident peaks is the approximate methodology used to take into account angular correlations. Angular correlations are usually at either a maximum or minimum at 180°°. The integrated-across solid angle angular correlations will necessarily be lower than the ones used in the data, which may reduce the variance in the data. The final averaged experimental ^{140}La activity was determined to be 585(65) Bq. This value was taken as simply the average of the activities for each coincidence. Due to the somewhat skewed nature of the ^{140}La activities for each coincident photopeak, average experimental activity uncertainty was taken as the population standard deviation. The SCALE and experimental ^{140}La agree within uncertainty, with the SCALE generated average ^{140}La activity of 657(138) Bq. This constitutes an 11% difference. Due to the high uncertainty associated with the initial ^{235}U in the sample, it is difficult to determine if the results are accurate or inaccurate. Future experiments will utilize enriched ^{235}U foils containing well characterized initial amounts of ^{235}U. With these results, experimental bias can be more readily determined.

Table 5 depicts a comparison between the coincidence spectrum and the spectrum generated via a single detector which can be seen in Figure 24. The coincidence criterion, developed in the in Chapter 1 and depicted in Eq. 17, indicate the background to net photo-peak area ratios which must be attained in order for coincidence methodologies to yield better accuracy. For ^{140}La, the most intense γ-ray occurs at 487 keV. From Table 5,

the background must have a magnitude 39 times greater than the net photopeak counts in order to warrant coincidence counting with the detectors studied. However, note that in almost all cases, detection limits are improved via coincidence methodologies. For the case of the 487 keV γ-ray, the detection limit has improved by 33% due to coincidence procedures. This demonstrates the advantage of coincidence counting: low-activity signatures can be extracted from high-backgrounds.

Table 5: Comparison of coincidence and single detector performance

		Detection limits	
Coincidence [keV]	Coincidence criterion	Coincidence MDA [Bq]	Single detector MDA [Bq]
[487 328]	39	1.2	1.8
[328 487]	25	1.5	3.2
[1596 487]	14	0.6	6.0
[487 1596]	75	0.2	1.8
[1596 328]	85	1.6	2.5
[328 1596]	85	1.0	3.2
[1596 815]	43	0.4	6.0
[815 1596]	78	0.4	1.5
[432 487]	20	5.4	23.0
[487 432]	317	4.7	1.8

It is also noteworthy that the HPGe detectors employed in this study have relatively low certified relative efficiencies. Eq. 10 indicates that the ratio of coincidence performance to single-detector performance is roughly proportional to detector efficiency. If two thicker and wider detectors are utilized, then the coincidence criterion may drop considerably. Further, if conducting field-work with compound room-temperature semi-conductors or scintillators with poorer resolution, then coincidence

methodologies become more applicable due to the increased background to net photo-peak area ratios.

Conclusions

The 11% difference between the modelled and experimental ^{140}La activities gives confidence to the present methodology. While it is difficult to determine the validity of the SCALE and PoliMi models to yield precise results in a radiochemistry lab setting, the results have proved the model's capability to predict γ-γ coincidence performance for the radiochemistry analysis of fission-products or other isotopes relevant to nuclear non-proliferation and stockpile stewardship. It was demonstrated that for the inefficient detectors employed in the present study, the background must be about 39 times higher than the net photo-peak area of the 487 keV γ-ray in order to warrant coincidence counting methodologies. Future work will entail further validating model performance by analyzing enriched uranium foils and developing a comprehensive list of coincidence performance for many of the isotopes relevant to nuclear non-proliferation and stockpile-stewardship. In this future work, models of the most efficient detectors on the market will be utilized to give an upper bound, or the best possible case, for coincidence performance.

Chapter 5: ^{239}Pu analysis

Abstract

This chapter presents an experiment to determine the viability of γ coincidence methodologies to determining ^{239}Pu concentrations applicable to stockpile stewardship operations. A plutonium foil was counted for two days in the two detector HPGe system outlined in Chapters 3 and 4. By comparing the single detector spectrum to the coincidence spectrum, coincidence criteria were generated for the 18 most intense coincidences in the ^{239}Pu spectrum.

Experimental and results

A 1 cm diameter nickel-plated Pu plutonium foil was counted 2 cm from each detector endcap for two days. The enclosed PuO_2 weighed 0.899 mg and had a 99.36% ^{239}Pu, 0.63% ^{240}Pu, and 0.01% ^{241}Pu isotopic comosition. An image of the multiple coincidences between various γ-rays and x-rays spanning 90 to 205 keV is depicted in Figure 25. The single spectrum from the portable detector depicts that one advantage of coincidence counting with ^{239}Pu is the capability of counting coincidences between the x-rays generated from internal conversion events and γ-rays. Counting these x-rays alone in a single detector system may introduce a bias since other Pu isotopes will emit similar x-ray energies. With two detectors, the x-rays will be in coincidence with definitive γ signatures from ^{239}Pu.

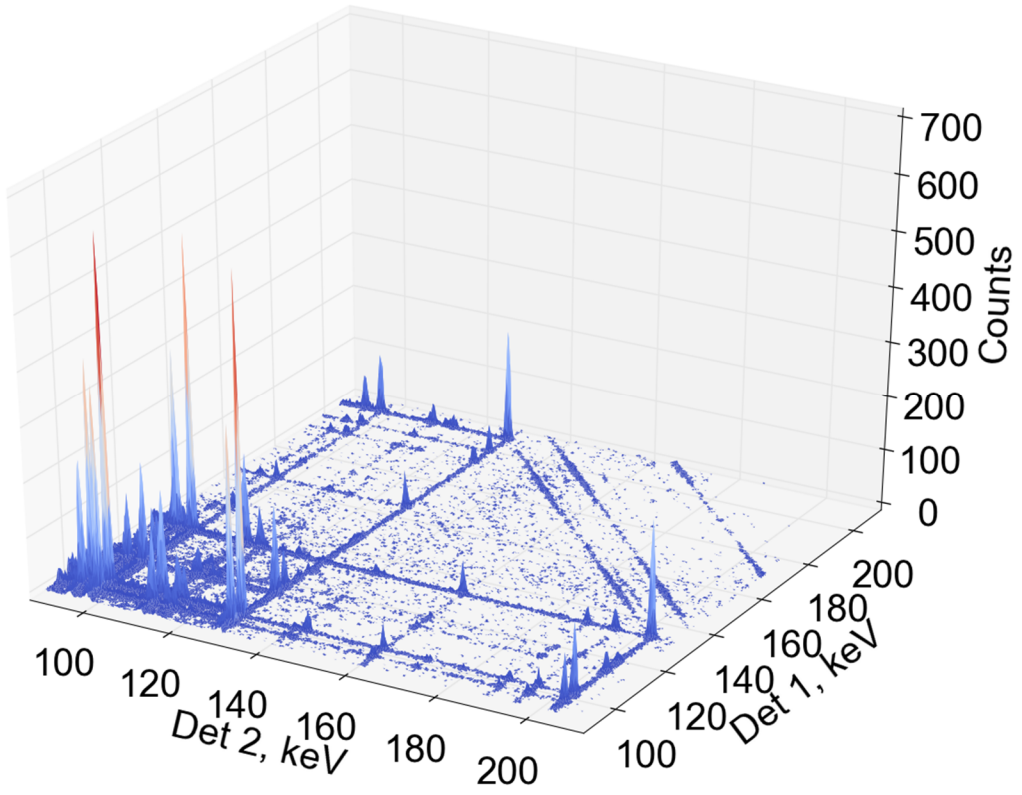

Figure 25: Coincidences of ^{239}Pu

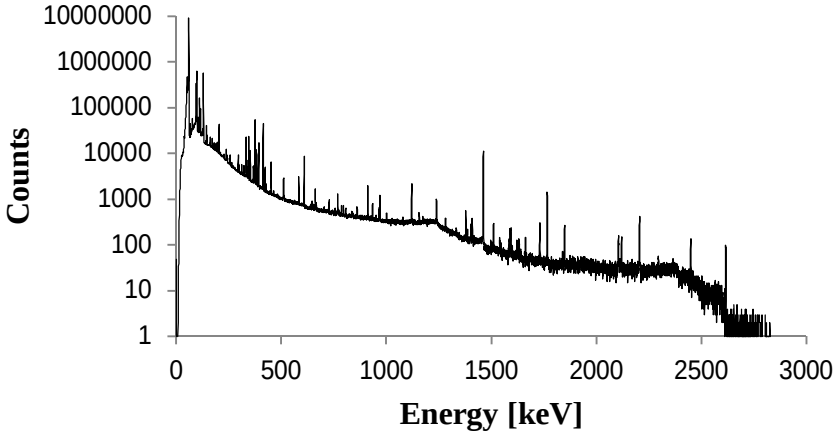

Figure 26: ^{239}Pu and ^{241}Am singles spectrum from Pu foil

The results of the coincidence and singles spectral analysis is depicted in Table 6.

Table 6: Results of ^{239}Pu analysis[6]

Coincidence [keV]	Particle type	Coincidence counts	Coincidence criterion	Normal MDA/Coincidence MDA
[203.6-129.3]	γ-γ	1735(42)	28	1.42
[129.3-203.6]	γ-γ	1815(43)	415	0.15
[195.7-203.6]	γ-γ	361(19)	31	1.83
[129.3-195.7]	γ-γ	336(19)	2243	0.04
[203.6- 94.7]	γ-kα2	681(26)	73	0.87
[94.7-203.6]	kα2-γ	765(28)	550	0.24
[161.5-129.3]	γ-γ	494(23)	27	1.96
[129.3-161.5]	γ-γ	466(22)	1617	0.05
[129.3-115]	γ-(γ+kβ2)	748(28)	1007	0.06
[115-129.3]	(γ+kβ2)-γ	756(29)	296	0.14
[129.3-111.3]	γ-kβ1	2032(46)	371	0.11
[111.3-129.3]	kβ-γ	2003(46)	134	0.30
[129.3-98.8]	γ-(γ+kα1)	4637(68)	162	0.32
[98.8-129.3]	(γ+kα1)-γ	5018(72)	172	0.30
[129.3-94.7]	γ-kα2	3195(58)	235	0.14
[94.7-129.3]	kα2-γ	3378(58)	124	0.54
[98.4-203.6]	(γ+kα1)-γ	1162(34)	745	0.10
[203.6-98.4]	γ-(γ+kα1)	1064(33)	47	1.23

The ^{239}Pu γ-ray with the most counts in the single detector spectrum without an x-ray interference is at 129.3 keV. The best coincidence containing the 129.3 keV γ-ray is [129.3 98.8] keV, where the 98.8 keV signal contains both a kα1 x-ray at 98.4 and a γ-ray at 98.8 keV whose energies are within the resolution of the detectors. The coincidence

[6] All uncertainties in parentheses are one-sigma

criterion for this coincidence is very high at 162. Therefore, background levels would have to be 162 times higher than the net photo-peak area in the single detector spectrum to warrant coincidence techniques. If more efficient detectors are used, then the criterion may improve. However, due to the close geometries used in this experiment, increasing crystal width may not significantly increase the solid angles subtending the source and crystal faces. Therefore, using larger detectors may not generate significantly higher efficiencies at the low energies characteristic of ^{239}Pu analysis where crystal depth does not come significantly into play. Other coincidences have similar poor coincidence criteria. Further, detection limits are on average 50% lower for coincidence counting.

The most abundant x-rays associated with the decay of ^{239}Pu consist of the L x-rays ranging in energy from 11 to 21 keV. Due to high sample density, thick aluminum casing, and significant dead-layer thickness, the majority of these x-rays were not detected. Therefore, these results do not take into account the potential benefit from the detection of these x-rays in a system with higher efficiency at those low energies.

Conclusions

Coincidence counting of ^{239}Pu yielded additional isotopic signatures in the form of x-ray - γ coincidences which allow the coincidence methodology to utilize more photo-peaks for isotopic activity determination. However, poor coincidence efficiencies led to poor coincidence performance in relation to the conventional γ-spectroscopy methodology.

Chapter 6: Closing remarks

Conclusions

This thesis has presented the theory of γ-coincidence counting including discussions on determining coincidence efficiencies, angular-correlations, dead-time, and effects due to random coincidence summing. A simple, dimensionless parameter independent of counting time has been proposed in order to quantitatively determine the benefit of implementing γ-coincidence techniques. This coincidence criterion specifies the noise-to-signal ratio necessary for a γ coincidence system to outperform a single-detector system: $\frac{B}{P_\gamma} > \frac{\alpha-1}{2}\frac{B}{P_\gamma} > \frac{\alpha-1}{2}$ where α is the ratio of the coincidence efficiency to single photo-peak efficiency. If the radiochemist operating a single γ detector typically encounters photo-peaks with noise-to-signal ratios higher than this criterion, then a coincidence system with similar detectors will yield a more precise result in the same count duration. Coincidence counting can also have the additional benefit of removing interferences which may be present in complex fission-product spectra. This additional benefit is not included in the coincidence criterion.

The capability of γ coincidence counting to generate precise results in a laboratory environment with the use of known standards was demonstrated with the determination of selenium in activated fly-ash. Experimentally determined selenium concentations agreed very well with the certified values in the reference materials. This experiment

further demonstrated the capability of coincidence counting to eliminate interferences in complex spectra encountered, for example, in the determination of fission products in spent nuclear fuel. A methodology to correct for random-coincidences via post-processing of the list mode data was also presented. Further, this thesis presented two separate methodologies to correct for dead-time, one experimental and one analytical. The virtual complete elimination of natural background in a coincidence system was also demonstrated. This adds the additional benefit of potentially eliminating the need for dense metal shielding surrounding the detection system.

A first-iteration Monte Carlo model was developed in order to determine coincidence efficiencies when standards with the exact geometry and matrix of the sample are not readily available. A uranium solution was irradiated in the TRIGA Mark II reactor to simulate spent nuclear fuel. Experimentally determined ^{140}La activity using coincidence intensities generated from the PoliMi model agreed within uncertainty with the prediction from the SCALE activation model. The capability to determine model precision was hindered by the high uncertainty associated with the initial ^{235}U value. However, the model proved sufficiently accurate to be used as a tool to assess the potential benefit of γ-γ coincidence in the determination of fission product concentrations.

The benefit of γ-γ-coincidence counting to the determination of ^{239}Pu content was experimentally assessed. While γ-γ coincidence proved capable of extracting additional

photo peaks containing x-ray–γ coincidences, the calculated coincidence criterion of 162 indicates a relatively small potential benefit of using a HPGe coincidence system for the determination of ^{239}Pu. However, these results do not take into account the potential benefit of utilizing larger, more efficient HPGe crystals. Further, they do not take into account the potential benefit of using thin C or Be windows in order to detect the more abundant L x-rays with energies ranging from 11 to 21 keV.

This thesis attempts to define applicable situations for γ-γ coincidence techniques. Coincidence techniques are most valid when attempting to find a small peak underneath a large background containing multiple spectral interferences. Compound room-temperature semiconductor detectors and scintillators have poorer resolution than HPGe detectors. As resolution decreases, the background underneath a photo-peak gets larger and larger. Taking this under consideration, room-temperature detectors may benefit more from γ-γ-coincidence as long as interferences are not encountered from other coincidences with close energies. While it has been demonstrated that γ-γ coincidence is certainly capable of generating precise results in a laboratory environment if certified standards are present, the complexity associated with obtaining coincidence efficiencies, combined with the dependence on the accuracy of tertiary particle information contained in the nuclear data, makes it difficult to obtain ultra-precise results without these standards. Combining all of these points together leads to potential applications which may be very suitable for coincidence counting: the detection of minute traces of fission-

products and other isotopes relevent to non-proliferation in high-activity nuclear materials in the field using portable room-temperature detectors. Coincidence will likely remove the majority of the background and interferences in these samples and can quickly determine go / no-go criteria in binary decision-making scenarios. Coincidence counting will further help to mitigate the lack of precision due to the poorer resolution associated with these detectors.

Future work

It is proposed to further validate the PoliMi model by counting irradiated enriched U foils with more precise concentrations of ^{235}U. Further, a more detailed angular-correlation correction model will be developed which integrates over the solid angles subtending the source and detector faces. Using this validated model, the coincidence efficiencies and coincidence criteria will then be generated for a large number of fission products and actinides relevent to non-proliferation and stockpile stewardship applications. It is also proposed to utilize models of the most efficient detectors currently on the market to generate upper-bounds on coincidence performance for all of the isotopes studied. It is also proposed to examine coincidence performance for room-temperature detectors in field-situations.

Appendix A: coincidence intensity MCNP code

```
HPGe Detector Input Deck
c cell cards
2 2 -0.001205 -1 #(-103 2 -115) #(-3 -19 15) #201 #401 #501 IMP:P=1 imp:e=1 $ AIR
3 0 1 IMP:P=0  imp:e=0 $ VOID OUTSIDE
5 4 -2.698 -3 15 -19 #(16 -4 -19) IMP:P=1 imp:e=1 $ Aluminum Housing (R)
8 4 -2.698 -12 13 38 -20 #4 #6 #7 #9 #10 IMP:P=1 imp:e=1 $ Crystal Holder (R)
7 5 -5.323 -13 14 8 -18 #4 #6 #9 #10 IMP:P=1 imp:e=1 $ Outer Electrode (R)
4 7 -1.380 -12 48 -28 IMP:P=1 imp:e=1 $ Mylar Film in IR Window (R)
11 8 -1.420 -12 28 -38 IMP:P=1 imp:e=1 $ Kapton Layor in IR Window (R)
 13 5 -5.323 -13 38 -8 IMP:P=1 imp:e=1 $ Window Electrode (R)
 14 4 -2.698 -12 5 -48 IMP:P=1 imp:e=1 $ Aluminum Coating (R)
6 5 -5.323 -14 8 -18 #(-23 24 -18) #9 #10 IMP:P=1 imp:e=1 $ HPGe Crystal (R)
9 0 (-23 25 24 -18):(-13 25 18 -20):(16 -5 -4):(-4 12 5 -20)&
:(-4 20 -19) #12 imp:e=1 IMP:P=1 $ Vacuum Well (R)
10 6 -8.96 -25 24 -20 imp:p=1 imp:e=1 $ CuElectroinc (R)
12 9 -2.250 (-12 20 -27):(-29 20 -30) imp:p=1 imp:e=1 $ Teflon Insulator (R)
105 4 -2.698 -103 -115 2 #(-116 -104 2) IMP:P=1 imp:e=1 $ Aluminum Housing (L)
108 4 -2.698 -112 113 -138 120 #104 #106 #107 #109 #110 IMP:P=1 imp:e=1 $ Crystal Holder
(L)
107 5 -5.323 -113 114 -108 118 #104 #106 #109 #110 IMP:P=1 imp:e=1 $ Outer Electrode (L)
104 7 -1.380 -112 -148 128 IMP:P=1 imp:e=1 $ Mylar Film in IR Window (L)
111 8 -1.420 -112 -128 138 IMP:P=1 imp:e=1 $ Kapton Layor in IR Window (L)
 113 5 -5.323 -113 -138 108 IMP:P=1 imp:e=1 $ Window Electrode (L)
 114 4 -2.698 -112 -105 148 IMP:P=1 imp:e=1 $ Aluminum Coating (L)
106 5 -5.323 -114 -108 118 #(-123 -124 118) #109 #110 IMP:P=1 imp:e=1 $ HPGe Crystal (L)
109 0 (-123 25 -124 118):(-113 25 -118 120):(-116 105 -104)&
:(-104 112 -105 120):(-104 -120 2) #112 IMP:P=1 imp:e=1 $ Vacuum Well (L)
110 6 -8.96 -25 -124 120 imp:p=1 imp:e=1 $ CuElectroinc (L)
112 9 -2.250 (-112 -120 127):(-29 -120 130) imp:p=1 imp:e=1 $ Teflon Insulator (L)
201 10 -1.19 -202 201 -203 301 #(-103 -204 201) imp:p=1 imp:e=1 $ Sample Holder
401 11 -0.9998 -401 imp:p=1 imp:e=1 $ Sample
501 12 -7.82 -1 -501 imp:p=1 imp:e=1 $ Table

c surface cards
1 BOX 12.9 -13.69 -33.0 23.0 0 0 0 27.38 0 0 0 66.0 $ Air Box
2 PX 12.9 $ Back of Detector surface (L)
3 CX 3.805 $ Outer radius of Detector Housing (R)
4 CX 3.655 $ Inner radius of Detector Housing (R)
 5 PX 25.65 $ Front of IR Window (R)
 8 PX 25.766047 $ Front of HPGe (R)  - optimized dead layer
 12 CX 2.826 $ Outside of Crystal Holder (R)
 13 CX 2.75 $ Inside of Crystal Holder/Outside of Ge (R)
 14 CX 2.645 $ Crystal Diameter (R)  - optimized dead layer
 15 PX 25.0 $ Front of Aluminum Housing (R)
 16 PX 25.15 $ Back/Inside of Aluminum Housing (R)
18 PX 30.611047 $ Back of HPGe (R)
19 PX 35.90 $ Back of Aluminum Housing (R)
20 PX 32.861047 $ Back of Vacuum Well Inside Aluminum Housing (R)
 23 CX 0.4 $ Core Hole in Ge Radius (R)
24 PX 27.111047 $ Front of Core Hole (R)
 25 CX 0.2 $ Cu Electronic Radius (R)
27 PX 33.181047 $ Back of Crystal Holder (R)
 28 PX 25.650847 $ Back of Mylar Film in IR Window (R)
 38 PX 25.661047 $ Back of IR Window (R)
 48 PX 25.650050 $ Back of Aluminum Coating (R)
29 CX 1.2 $ Radius of Teflon Insulator (R)
30 PX 34.8 $ Back of Teflon Insulator (R)
103 CX 3.86 $ Outer radius of Detector Housing (L)
```

```
104 CX 3.71 $ Inner radius of Detector Housing (L)
 105 PX 21.35 $ Front of IR Window (L)
 108 PX 21.17962658  $ Front of HPGe (L)  - optimized dead layer
 128 PX 21.349153 $ Back of Mylar Film in IR Window (L)
 138 PX 21.338953 $ Back of IR Window (L)
 148 PX 21.349950 $ Back of Aluminum Coating (L)
 112 CX 2.701 $ Outside of Crystal Holder (L)
 113 CX 2.625 $ Inside of Crystal Holder/Outside of Ge (L)
 114 CX 2.465673575 $ Crystal Diameter (L) - optimized dead layer
 115 PX 22 $ Front of Aluminum Housing (L)
 116 PX 21.85 $ Back/Inside of Aluminum Housing (L)
 118 PX 18.088953 $ Back of HPGe (L)
 120 PX 15.838953 $ Back of Vacuum Well Inside Aluminum Housing (L)
123 CX 0.35 $ Core Hole in Ge Radius (L)
 124 PX 19.988953 $ Front of Core Hole (L)
 127 PX 15.518953 $ Back of Crystal Holder (L)
 130 PX 13.90 $ Back of Teflon Insulator (L)
201 PX 19.42 $ Left Surface of Sample Holder
202 CX 4.45 $ Outer Radius of Sample Holder
 203 PX 24.925 $ Sample Holder Right Surface
204 PX 22.075 $ Sample Holder Left Surface
 301 RCC 23.5 -2.53 0 0 6.98 0 0.8725 $ Hole in Sample Holder
 401 RCC 23.5 -1.11 0 0 1.245 0 0.4625 $ Sample
501 PY -12.38 $ Steel Table Surface

c source specification
SDEF CEL=401 PAR=SP ERG=0.0 POS= 23.595 -1.11 0 AXS 0 1 0 RAD D1 EXT D2
SI1 0 0.4625
SP1 0 1
SI2 0 1.245
SP2 0 1
act DG=LINES
F8:P 6
F18:P 6
F28:P 106
F38:P 106
FT18 GEB 0.00073568688 0.00085954495 0.48984239
FT38 GEB 0.00073568688 0.00085954495 0.48984239
E0 0.0 5190I 2.01
E8 0.0 5190I 2.01
E18 0.0 5190I 2.01
E28 0.0 5190I 2.01
E38 0.0 5190I 2.01
M2 6000 -0.000124 &
7000 -0.755268 &
8000 -0.231781 &
18000 -0.012827 $ Dry Air ICRU
M4 13000 -1 $ Aluminium
M5 32000 -1 $ Pure Germanium Crystal
M6 29000 -1 $ Copper Electroinc
M7 1000 -0.041960 &
6000 -0.625016 &
8000 -0.333024 $ Mylar Film
M8 1000 -0.026362 &
6000 -0.691133 &
7000 -0.073270 &
8000 -0.209235 $ Kapton
M9 6000 -0.240183 &
9000 -0.759818 $ Teflon Insulator
M10 1000 -0.080538 &
6000 -0.599848 &
8000 -0.319614 $ Lucite(Acrylic)
M11 1000 -0.11 &
```

```
8000 -0.88 &
92000 -0.01 $ Uranium Sample
M12 6000 -0.005 &
26000 -0.995 $ Steel, Carbon
MODE P
PHYS:P
NPS 1000000
```

References

1. Kobya Y, Taşkın H, Yeşilkanat C, Varinlioğlu A, Korcak S (2015) Natural and artificial radioactivity assessment of dam lakes sediments in Çoruh River, Turkey. J Radioanal Nucl Chem 303 (1):287-295

2. Karadeniz Ö, Yaprak G (2008) Geographical and vertical distribution of radiocesium levels in coniferous forest soils in Izmir. J Radioanal Nucl Chem 277 (3):567-577

3. Bandstra MS, Vetter K, Chivers DH, Aucott T, Bates C, Coffer A, . . . Yee B Measurements of Fukushima fallout by the Berkeley Radiological Air and Water Monitoring project. In: Nuclear Science Symposium and Medical Imaging Conference (NSS/MIC), 2011 IEEE, 23-29 Oct. 2011 2011. pp 18-24

4. BE Marie-Martine CN, Duchemin N., Lagoutine F., Legrand J., Debertin K., Schonfeld E. (2011) Introduction to table of nuclides. Laboratoire National Henri Becquerel.

5. C. B (2008) Chart of Nuclides. Available via National Nuclear Data Center. http://www.nndc.bnl.gov/chart/. Accessed 2015

6. Padgett S, Wang T-F (2015) Simulating γ–γ coincidences of β-delayed γ-rays from fission product nuclei. Nucl Instrum Meth A 770 (0):218-224

7. Penttilä H, Elomaa VV, Eronen T, Hakala J, Jokinen A, Kankainen A, . . . Äystö J (2012) Fission yield studies at the IGISOL facility. Eur Phys J A 48 (4):1-11

8. Agarwal C, Danu LS, Gathibandhe M, Goswami A, Biswas DC (2014) Coincidence summing corrections for a clover detector. Nucl Instrum Meth A 763 (0):240-247

9. D.S. Andreev KIE, V.S. Lemberg (1972) Consideration of cascade transitions in determining the absolute yield of gamma rays. instrum Exp Tech+ 15

10. McCallum GJ, Coote GE (1975) Influence of source-detector distance on relative intensity and angular correlation measurements with Ge(Li) spectrometers. Nucl Instrum Methods 130 (1):189-197

11. Korun M, Martinčič R (1993) Coincidence summing in gamma and X-ray spectrometry. Nucl Instrum Meth A 325 (3):478-484

12. Novković D, Kandić A, Đurašević M, Vukanac I, Milošević Z, Nađđerđ L (2007) Coincidence summing of X- and γ-rays in γ-ray spectrometry. Nucl Instrum Meth A 578 (1):207-217

13. Novković D, Đurašević M, Kandić A, Vukanac I, Milošević Z, Nađđerđ L (2007) Coincidence summing of X- and gamma rays of 133Ba. Nucl Instrum Meth A 582 (2):592-602

14. Sima O, Arnold D (2008) A tool for processing decay scheme data that encompasses coincidence summing calculations. Appl Radiat Isotopes 66 (6–7):705-710

15. Kanisch G, Vidmar T, Sima O (2009) Testing the equivalence of several algorithms for calculation of coincidence summing corrections. Appl Radiat Isotopes 67 (10):1952-1956

16. R. S (2001) Algorithms in C, Part 5: Graph Algorithms. 3 edn. Addison Wesley Professional,

17. Vidmar T, Likar A (2005) Calculation of total efficiencies of extended samples for HPGe detectors. Nucl Instrum Meth A 555 (1–2):251-254

18. Korun M (2004) Measurement of peak and total efficiencies of low-energy gamma-ray detectors with sources emitting photons in cascade. Appl Radiat Isotopes 60 (2–4):207-211

19. Blaauw M, Gelsema SJ (2003) Cascade summing in gamma-ray spectrometry in marinelli-beaker geometries: the third efficiency curve. Nucl Instrum Meth A 505 (1–2):311-315

20. Hamilton DR (1940) On Directional Correlation of Successive Quanta. Phys Rev 58 (2):122-131

21. Di Piero A, Bacchi MA, Fernandes EAN (2008) J Radioanal Nucl Chem 278 (3):761-765

22. Horne S, Landsberger S (2012) J Radioanal Nucl Chem 291 (1):49-53

23. Wangen LE, Gladney ES, Starner JW, Hensley WK (1980) Analytical Chemistry 52 (4):765-767

24. Ihantola S (2013). Applied Physics, vol Doctor of Science (Technology). Aalto University, Helsinki

25. Andersen O, Garrett JD, Hagemann GB, Herskind B, Hillis DL, Riedinger LL (1979) Physical Review Letters 43 (10):687-690

26. Pattabiraman NS, Ghugre SS, Basu SK, Garg U, Ray S, Sinha AK, Zhu S (2006) Nuclear Instruments and Methods in Physics Research Section A: Accelerators, Spectrometers, Detectors and Associated Equipment 562 (1):222-229

27. Westphal GP, Jöstl K, Schröder P, Lauster R, Hausch E (1999) Nuclear Instruments and Methods in Physics Research Section A: Accelerators, Spectrometers, Detectors and Associated Equipment 422 (1–3):347-351

28. Westphal GP (1998) Nuclear Instruments and Methods in Physics Research Section A: Accelerators, Spectrometers, Detectors and Associated Equipment 416 (2–3):536-538

29. Wiernik M (1971) Nuclear Instruments and Methods 96 (2):325-329

30. Hennig W, Chu YX, Tan H, Fallu-Labruyere A, Warburton WK, Grzywacz R (2007) Nuclear Instruments and Methods in Physics Research Section B: Beam Interactions with Materials and Atoms 263 (1):175-178

31. Steven H (2011) Advances in gamma-ray spectroscopy: compton suppression and gamma-gamma coincidence. The University of Texas at Austin,

32. Steven H (2013) Multispectral gamma-ray analysis using clover detectors with application to uranium fission product analysis. The University of Texas at Austin,

33. Jordan W (2011) Development of PYRAMIDS (Python for Radioisotope Analysis and Multi-Detector Suppression) code used in fision product detection limit improvements with the DGF Pixie-4 digital spectrometer. The University of Texas at Austin,

34. Currie LA (1968) Limits for qualitative detection and quantitative determination. Application to radiochemistry. Analytical Chemistry 40 (3):586-593

35. User's manual digital gamma finder (DGF) Pixie-4 (2013).

36. Gilmore GR (2008) Appendix D: Gamma-Ray Energies in the Detector Background and the Environment. In: Practical Gamma-Ray Spectrometry. John Wiley & Sons, Ltd, pp 361-364

37. Popov YS, Kazarinov NM, Popov VY, Rykov YM, Skirda NV (2005) Measuring Low Activities of Fission-Product Xenon Isotopes Using the β-γ Coincidence Method. Instrum Exp Tech+ 48 (3):380-386

38. Cox CE, Hennig W, Huber AC, Warburton WK, Grudberg PM, Asztalos SJ, . . . Biegalski S A 24-element Silicon PIN diode detector for high resolution radioxenon measurements using simultaneous X-ray and electron spectroscopy. In: Nuclear Science Symposium and Medical Imaging Conference (NSS/MIC), 2013 IEEE, Oct. 27 2013-Nov. 2 2013 2013. pp 1-7

39. Zhang W, Mekarski P, Lam J, Ungar K, Pellerin E (2010) Geant4 Monte Carlo radioxenon beta-gamma coincidence efficiency simulation for a phoswich detector. J Radioanal Nucl Chem 285 (3):475-482

40. Peerani P, Carbol P, Hrnecek E, Betti M (2002) Assessment of a Compton-event suppression γ-spectrometer for the detection of fission products at trace levels. Nucl Instrum Meth A 482 (1–2):42-50

41. Bender S (2014) Study of Compton suppression for use in spent nuclear fuel assay. Ph.D., The Pennsylvania State University, Ann Arbor

42. Kane S, Gozani T, King MJ, Kwong J, Brown C, Gary C, . . . McKinsey DN (2013) Simulations of Multi-Gamma Coincidences From Neutron-Induced Fission in Special Nuclear Materials. Nucl Sci IEEE Transactions 60 (2):533-538

43. Miller E, S. C, Flaska M, Prasad S, Pozzi S, Padovani E (2012) MCNPX-PoliMi post-processing algorithm for detector response simulations. J Institute Nucl Mat Management 40 (2):34

44. Pozzi SA, Clarke SD, Flaska M, Peerani P (2009) Pulse-height distributions of neutron and gamma rays from plutonium-oxide samples. Nucl Instrum Meth A 608 (2):310-315

45. Clarke SD, Pozzi SA, Flaska M, Downar TJ (2009) Monte Carlo study of photoneutron production in U-235 following perturbations in cross section data. Ann Nucl Energy 36 (3):393-398

46. Miller EC, Dennis B, Clarke SD, Pozzi SA, Mattingly JK (2011) Simulation of polyethylene-moderated plutonium neutron multiplicity measurements. Nucl Instrum Meth A 652 (1):540-543

47. Hull EL, Pehl RH, Madden NW, Luke PN, Cork CP, Malone DL, . . . Friesel DL (1995) Temperature sensitivity of surface channel effects on high-purity germanium detectors. Nucl Instrum Meth A 364 (3):488-495

48. Ashrafi S, Likar A, Vidmar T (1999) Precise modeling of a coaxial HPGe detector. Nucl Instrum Meth A 438 (2–3):421-428

49. Elanique A, Marzocchi O, Leone D, Hegenbart L, Breustedt B, Oufni L (2012) Dead layer thickness characterization of an HPGe detector by measurements and Monte Carlo simulations. Appl Radiat Isotopes 70 (3):538-542

50. Huy NQ (2011) Dead-layer thickness effect for gamma spectra measured in an HPGe p-type detector. Nucl Instrum Meth A 641 (1):101-104

51. Huy NQ, Binh DQ, An VX (2007) Study on the increase of inactive germanium layer in a high-purity germanium detector after a long time operation applying MCNP code. Nucl Instrum Meth A 573 (3):384-388

52. Boson J, Ågren G, Johansson L (2008) A detailed investigation of HPGe detector response for improved Monte Carlo efficiency calculations. Nucl Instrum Meth A 587 (2–3):304-314

53. Scale: A comprehensive modeling and simulation suite for nuclear safety analysis and design, ORNL/TM-2005/39, Version 6.1 (2011). Available from Radiation Safety Information Computational Center at Oak Ridge National Laboratory as CCC-785

54. Lamarsh JR (1983) Introduction to nuclear engineering. Addison-Wesley series in nuclear science and engineering, vol xiv, 689 p. Addison-Wesley, Reading, Mass.